JCTC Journal of Chemical Theory and Computation

pubs.acs.org/JCTC Article

Molecular Dynamics Approach to Calculate the Thermodiffusion (Soret and Seebeck) Coefficients of Salts in Aqueous Solutions

Leandro Rezende Franco,* André Luiz Sehnem,* Antônio Martins Figueiredo Neto,* and Kaline Coutinho*

Cite This: J. Chem. Theory Comput. 2021, 17, 3539−3553 Read Online

ACCESS | Metrics & More | Article Recommendations | Supporting Information

ABSTRACT: An approach to investigate the physical parameters related to ion thermodiffusion in aqueous solutions is proposed herein by calculating the equilibrium hydration free energy and the self-diffusion coefficient as a function of temperature, ranging from 293 to 353 K, using molecular dynamics simulations of infinitely diluted ions in aqueous solutions. Several ion force field parameters are used in the simulations, and new parameters are proposed for some ions to better describe their hydration free energy. Such a theoretical framework enables the calculation of some single-ion properties, such as heat of transport, Soret coefficient, and mass current density, as well as properties of salts, such as effective mass and thermal diffusion, Soret and Seebeck, coefficients. These calculated properties are compared with experimental data available from optical measurements and showed good agreement revealing an excellent theoretical predictability of salt thermodiffusion properties. Differences in single-ion Soret and self-diffusion coefficients of anions and cations give rise to a thermoelectric field, which affects the system response that is quantified by the Seebeck coefficient. The fast and slow Seebeck coefficients are calculated and discussed, resulting in values with mV/K order of magnitude, as observed in experiments involving several salts, such as K^+Cl^-, Na^+Cl^-, H^+Cl^-, Na^+OH^-, TMA^+OH^-, and TBA^+OH^-. The present approach can be adopted for any ion or charged particle dispersed in water with the aim of predicting the thermoelectric field induced through the fluid. It has potential applications in designing electrolytes for ionic thermoelectric devices in order to harvest energy and thermoelectricity in biological nanofluids.

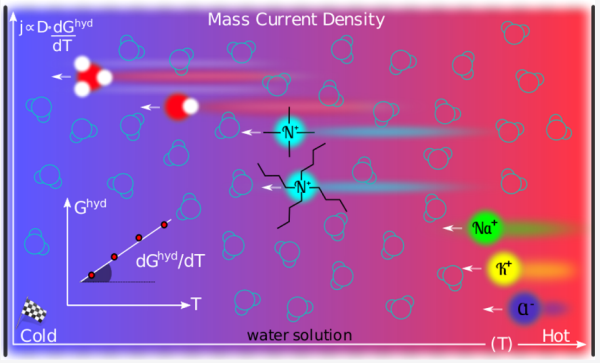

1. INTRODUCTION

The need to increase and diversify the world energy matrix has lead to the emergence of research on multiple energy sources, including low-grade harvesting devices with optimized thermoelectric response.[1,2] In liquid electrolytes or ionic liquids, there is a strong Seebeck effect, in which the electrostatic potential drop is induced by a temperature difference.[1,3] The thermoelectric energy is enhanced increasing the electrical conductivity σ and Seebeck coefficient S and decreasing the thermal conductivity κ of the fluid.[4] Aqueous electrolytes have a higher figure of merit (for efficiency assessment) when compared to nonaqueous electrolytes, mainly due to their higher σ values.[5] The Seebeck coefficient S of electrolytes depends on the single-ion Soret coefficient α_i, which is defined as the ratio of a concentration change in ions, or charged molecules or particles, induced by a temperature difference in aqueous solutions, that is, it depends on the tendency of spatial separation of negative and positive charge carries induced by the thermal gradient. Therefore, the Soret effect describes ionic diffusive motion that originates from a temperature gradient along its direction, defining the thermodiffusion effect.[6] It is different from self-diffusion, or tracer diffusion, which is a spontaneous random movement of particles (neutral or charged) in the absence of concentration (or chemical potential) gradient.

The single-ion Soret coefficient α_i is related to single-ion heat of transport or entropy of transport,[7] Q_i^* and S_i^*, respectively, arising from the temperature dependence upon interactions between ions and solvent molecules.[8] Knowledge on the underlying physical mechanisms, that is, the nature of specific interactions that drive charge carriers in temperature gradients, leads to an optimization of low-grade energy devices based on aqueous electrolytes, such as thermoelectric supercapacitors and thermopiles.[1,5,9] New electrolytes and ionic liquids are promising candidates to optimize such devices. However, even for the case of a monovalent and monoatomic salt dissociated in

Received: February 1, 2021
Published: May 4, 2021

https://doi.org/10.1021/acs.jctc.1c00116
J. Chem. Theory Comput. 2021, 17, 3539−3553

water, it is impossible to predict their performance at generating thermoelectric energy due to the absence of a thorough description of thermodiffusive effects.

The presence of temperature gradients in aqueous salty solutions induces an increasing ion concentration in the cold or hot side of the solution.[7,10,11] This is due to the thermodiffusion effect that generates an ionic flux which is generally given by the mass current density

$$j_{Ti} = -n_i \alpha_i D_i \nabla T / T \tag{1}$$

where $i = +$ for cations and $i = -$ for anions, n_i and D_i are the numerical volumetric concentrations and the self-diffusion coefficient of ion i, respectively, and ∇T is the temperature gradient. Accumulation of ions means that, in accordance with Fick law of diffusion, there is a counter-ion flux given by $j_{ni} = -D_i \nabla n_i$. Therefore, the single-ion Soret coefficient α_i characterizes ion thermodiffusion. The difference in α_i between the positive and negative ions has been assigned to generate charge accumulation. An electrostatic potential drop arises in the temperature gradient, for which the Seebeck coefficient is defined as the potential over the temperature differences. A first out-of-equilibrium thermodynamic description of the aforementioned effect was issued by Eastman nearly 100 years ago[12,13] who had proposed a relation between α_i and entropy of transport S_i^*. Agar et al. have related the salt Soret coefficient that is experimentally accessible[14,15] to the single-ion heat of transport Q_i^*.[8]

In recent years, scientific interest focused on experimental measurements to reveal elementary aspects of the Soret effect. The nature of ions[16−18] such as the hydrophilic/hydrophobic degree has an important role in driving solute migration toward the cold or hot side of the solution in temperature gradients.[19,20] Regarding electrolytes, differences in α_i[21] or Q_i^*[7] and in D_i[22] of anions and cations are predicted to generate a thermoelectric field, which leads to thermophoresis of charged nanoparticles[18,23−25] and it has been increasingly investigated so that it can be applied in energy harvesting.[1,2,26,27]

Some theoretical concepts of thermodiffusion in a given solution have been developed based on the temperature dependence of the particle free energy.[28−30] They considered a simple model where the solution was depicted in many thin-slab cells compared to the volume of the total solution but macroscopic compared to the particle size. From the reference cell at temperature T, neighbor cells are at different temperatures $T - \delta T$ and $T + \delta T$ toward cold and hot directions, respectively, in the temperature gradient. The probability of the particle movement to the neighboring cell is related to the change in entropy, thus causing absorption or heat release. This single-ion heat of transport Q_i^* was defined as $Q_i^* = T(\mathrm{d}G_i/\mathrm{d}T)$, where G_i is the Gibbs free energy of the single-ion/solvent system in local equilibrium. It is the basis for describing a nonequilibrium effect using equilibrium parameters. The single-ion Soret coefficient equation was defined as[12,30]

$$\alpha_i = \frac{Q_i^*}{2k_B T} = \frac{1}{2k_B}\frac{\mathrm{d}G_i}{\mathrm{d}T} \tag{2}$$

where the positive single-ion Soret coefficient α_i indicates the ion movement to the cold side through the temperature gradient. This equation has been applied in experimental results with charged microparticles by Duhr and Braun.[28]

Microscopic features of aqueous solutions that lead to the ionic Soret effect raises a fundamental question, that is, whether the calculation of ion free energy is enough to describe the ionic Soret effect and whether interactions other than electrostatic ones also play a major role.

Takeyama and Nakashima[31] showed proportionality between the single-ion heat of transport Q_i^* and ion hydration entropy, $Q_i^* = -f_i^{TN} T S_i^{hyd}$, using experimental data. Therefore, as eq 2 suggests, a starting point to describe the thermodiffusion of single ions in aqueous solution is to calculate the hydration free energy at different temperatures, $G_i^{hyd}(T)$, and obtain the ion hydration entropy as $-S_i^{hyd} = \mathrm{d}G_i^{hyd}/\mathrm{d}T$. Then, G_i^{hyd} of ions can be calculated by molecular dynamics (MD) simulations at the atomistic level under specific temperature conditions.

Carlsson and Åqvist[32] used MD simulations combined with the perturbation technique to calculate the hydration free energy G_i^{hyd} for the monoatomic cations (Li^+, Na^+, K^+, Rb^+, and Cs^+). Their results present a positive free energy variation by a temperature increase, $\Delta G_i^{hyd}/\Delta T > 0$, in which values of hydration free energy at 298 K are in good agreement with experimental data. Recently, Niether et al.[33,34] have analyzed the connection between hydrophilicity/hydrophobicity and thermodiffusion of biomolecules in aqueous solutions. These works suggest that the temperature dependence on the total interaction between ions and water molecules, which is calculated by $G_i^{hyd}(T)$, may be the most thorough physical description of the thermodiffusion of (molecular) ions and biomolecules. However, although there are some theoretical studies about the dependence of $G_i^{hyd}(T)$ on temperature in aqueous solutions and how it is associated with thermodiffusion, it is found that there is no calculation of thermodiffusion-related coefficients, such as the Soret coefficient (eq 2) using $G_i^{hyd}(T)$ calculated through computational methods. Lecce et al.[35,36] have recently performed computational simulations using nonequilibrium MD to calculate thermodiffusion coefficients of finite concentrations of Li^+Cl^- in aqueous solutions. Their computational approach calculates the heat of transport for anions and cations in each simulation, which requires multiple ions and thousands of water molecules for each simulation and demands long computational time. They reveal substantial differences between transport coefficients at infinite dilution and finite concentrations.

Therefore, MD simulations of infinitely diluted aqueous solutions of ions have been used in this work in order to evaluate the dependence on hydration free energy on temperature, $\Delta G_i^{hyd}/\Delta T$, using the Bennett acceptance ratio (BAR) method. We performed simulations for different types of ions in water, including the monoatomic alkali halide ions (Na^+, K^+, and Cl^-), the tetra-*n*-alkyl-ammonium (TAA) with $n = 1$ (tetramethylammonium, TMA^+) and 4 (Tetrabutylammonium, TBA^+), and hydronium H_3O^+ and hydroxide OH^- ions. We adopted two force field models for water and four force field parameters for monoatomic ions. For hydroxide and hydronium, we adopted available force field parameters, but we also propose a new set of nonbonded parameters for these ions in order to better reproduce their hydration free energies at room temperature. Moreover, we propose a new set of atomic charge distribution for *TAA* ions within the force field parameters. Additionally, we calculated ionic self-diffusion coefficients at different temperatures, $D_i(T)$, using the slope of mean square displacement (MSD). This extensive investigation offers a complete overview of the temperature dependence on the hydration and mobility of ions that have been used as basis to understand the microscopic structure of ions and thermodiffusion of salts. In this context, some single-ion properties were calculated, such as the Soret

https://doi.org/10.1021/acs.jctc.1c00116
J. Chem. Theory Comput. 2021, 17, 3539−3553

Table 1. Hydration Free Energies $G_i^{hyd}(T)$ (in kcal/mol) for Ions in Aqueous Solutions Calculated Using the BAR Method in MD Simulations at Different Temperatures with Different Force Field Parameters for Ions and the SPC/E Water Model[a]

ion	force field	G_i^{hyd} (293)	G_i^{hyd} (298)		G_i^{hyd} (313)	G_i^{hyd} (333)	G_i^{hyd} (353)
Cl^-	Canongia Lopes[44]	−104.2(1)	−103.8(1)	[−89.1][38]	−103.5(1)	−102.8(2)	−102.0(2)
	Dang[45]	−90.2(2)	−90.1(1)	[−81.3][39]	−89.7(1)	−89.2(2)	−88.8(1)
	Jorgensen[46]	−91.2(2)	−91.0(1)		−90.7(1)	−90.1(1)	−89.8(2)
	Roux[47]	−96.6(2)	−96.1(2)		−95.8(1)	−95.2(2)	−94.7(1)
K^+	Åqvist[48]	−64.4(1)	−64.4(2)	[−71.2][38]	−64.4(1)	−64.1(1)	−63.8(1)
	Dang[49]	−64.9(1)	−64.7(1)	[−70.5][39]	−64.4(1)	−64.4(2)	−64.2(1)
	Jorgensen[46]	−59.3(2)	−59.3(1)		−59.0(0)	−59.0(2)	−58.8(1)
	Roux[50]	−69.0(1)	−68.9(1)		−68.8(1)	−68.6(1)	−68.5(1)
Na^+	Åqvist[48]	−82.3(2)	−82.0(1)	[−88.7][38]	−81.9(1)	−81.6(1)	−81.2(1)
	Dang[45]	−89.2(1)	−89.0(1)	[−87.2][39]	−88.9(1)	−88.4(1)	−87.9(1)
	Jorgensen[46]	−76.7(1)	−76.5(1)		−76.2(1)	−76.1(1)	−75.8(1)
	Roux[50]	−91.8(2)	−91.6(1)		−91.3(1)	−90.8(0)	−90.2(1)
OH^-	Netz[51]	−124.4(1)	−124.1(2)	[−105.0][40]	−123.2(2)	−122.6(1)	−121.3(2)
	Jorgensen[46]	−130.0(3)	−129.9(3)		−128.9(2)	−127.6(1)	−126.8(2)
	20-sites[52]	−136.7(3)	−136.3(3)		−135.9(1)	−133.7(2)	−133.0(2)
	ours	−107.4(2)	−107.2(3)		−106.7(1)	−106.2(3)	−105.4(3)
H_3O^+	Netz[51]	−103.6(1)	−103.4(2)	[−110.4][40]	−102.8(1)	−101.9(2)	−101.1(2)
	ours	−110.7(3)	−110.5(1)		−109.6(3)	−108.6(3)	−108.0(3)
TMA^+	ours	−37.0(2)	−36.9(2)		−36.3(2)	−35.7(1)	−35.2(4)
TBA^+	ours	−26.3(4)	−26.1(3)		−24.6(2)	−23.2(3)	−22.1(3)

[a]The uncertainty of the last digit is in parenthesis and the experimental values at room temperature are in brackets.

coefficient α_i, heat of transport coefficient Q_i^*, and mass current density j_{Ti}, in addition to some salt properties, such as effective mass diffusion D, thermal diffusion coefficient D_T, and Soret S_T and Seebeck S coefficients.

A thermodiffusive interdependence between anions and cations is associated with the salt concentration gradient and the thermoelectric field arising along a temperature gradient in ionic solutions. An elementary source of ion thermodiffusion has been assumed according to different probabilities of moving toward the cold or hot side of the solution,[29,37] depending on the difference in hydration free energy. An investigation of ions was carried out based on a comparison of calculated values with experimental data available for $G_i^{hyd}(T)$ and α_i. From calculated α_i and D_i, we estimate the salt Soret S_T and Seebeck S coefficients of ionic solutions. The dependence of thermal diffusion coefficient D_T on temperature, a broadly discussed topic in the literature on thermodiffusion, shows a linear behavior with temperature as a consequence of the temperature independence of the single-ion Soret coefficient α_i and a linear dependence of effective mass diffusion $D(T)$ for all ions. For describing the thermoelectric effect, the Seebeck coefficient was calculated using a recent theoretical expression,[22] with agreements in the same orders of magnitude for monovalent salt in aqueous solutions. These analyses validate our procedure to computationally estimate thermodiffusion-related coefficients of charged molecules/particles in water and indicate the method to be used in the development of complex electrolytes for thermoelectric energy-harvesting devices.

2. RESULTS AND DISCUSSION

The results are going to be presented in four sections. First, those obtained from MD simulations are going to be shown in order to discuss their physical framework based on the hydration free-energy dependence on temperature for assessing the thermodiffusion effect in electrolyte solutions. Values of the hydration free energies $G_i^{hyd}(T)$ for ions obtained using different force field parameters are going to be presented and compared with available experimental data.[38−40] Next, ion self-diffusion coefficients $D_i(T)$ obtained from MD simulations for different temperatures will be presented, discussed, and compared with experimental data.[8,41] Additionally, the values calculated for salt effective mass diffusion $D(T)$ at different temperatures are shown, discussed, and compared with experimental data.[16,42] Then, the values calculated for single-ion properties: Soret coefficient α_i, heat of transport coefficient Q_i^*, and mass current density j_{Ti} are shown. The values calculated for the single-ion heat of transport Q_i^* are compared with experimental values obtained by Agar et al.,[8] and those for the single-ion mass current density j_{Ti} are discussed by showing a classification scale of ion thermodiffusion under the same concentration n_i and temperature gradient $\nabla T/T$ conditions. Finally, the calculated values for salt thermodiffusion-related coefficients, that is, thermal diffusion D_T and Soret S_T and Seebeck at fast and slow time regimes, S_{fast} and S_{slow}, respectively, are presented, discussed, and compared with experimental values obtained from optical experiments.[16,42,43]

2.1. Ion Hydration. The hydration free energy $G_i^{hyd}(T)$ for studied ions has been calculated at 13 different temperatures, in the range of 293−353 K in intervals of 5 K. In Table 1, the $G_i^{hyd}(T)$ values are shown only for five temperatures for simplification. We choose the four values equally spaced between the temperature interval (293, 313, 333, and 353 K) and additionally the room temperature (298 K) to compare with the most abundant data in the literature.[38−40] Different ionic force field parameters[44−52] are identified in the second column of Table 1 and their parameters are shown in the Supporting Information. In Table 1, only the results obtained for MD simulations using the SPC/E water model are presented. The results obtained using the TIP3P water model are presented in the Supporting Information.

As expected, all $G_i^{hyd}(T)$ are negative and alkyl ions, TBA^+ and TMA^+, are less hydrophilic than the others. The values calculated for TBA^+ and TMA^+ are $G_i^{hyd}(298)$ = −26.1 and −36.9 kcal/mol, respectively. As for K^+, the values of $G_i^{hyd}(298)$

https://doi.org/10.1021/acs.jctc.1c00116
J. Chem. Theory Comput. 2021, 17, 3539−3553

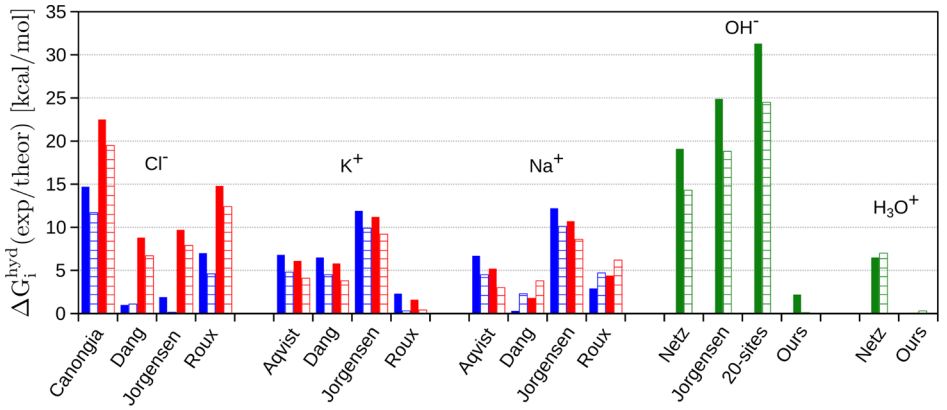

Figure 1. Experimental/theoretical differences of the hydration free energy, ΔG_i^{hyd}(exp/theor) at T = 298 K for different ionic force field parameters with two water models: SPC/E (solid bar) and TIP3P (open bar). The colors represent different experimental data presented by: Schmid et al.[38] (blue), Marcus[39] (red), and Pliego and Riveros[40] (green).

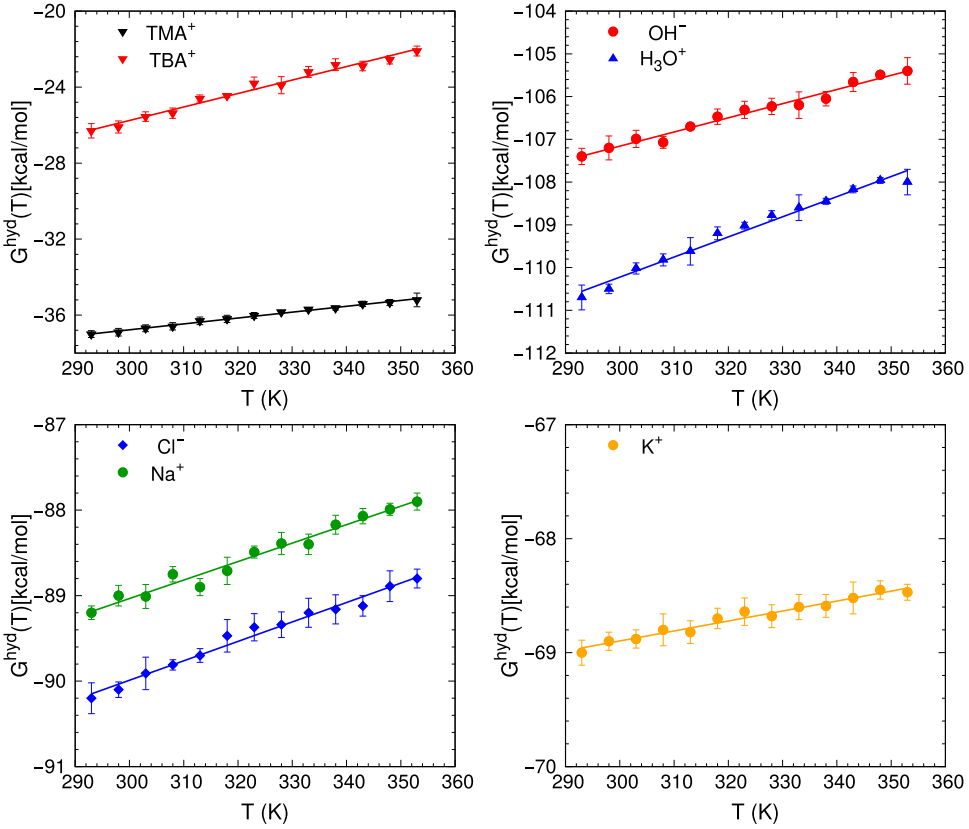

Figure 2. Hydration free energy $G_i^{hyd}(T)$ calculated for ions at temperatures ranging between 293 and 353 K using the BAR method in MD simulations using force field parameters with best experimental/theoretical agreement (Dang for Cl^- and Na^+, Roux for K^+, and ours for OH^-, H_3O^+, TMA^+, and TBA^+) and the SPC/E water model. The best linear fit is presented for each ion and its slope describes the ionic hydration entropy (in cal/mol·K), $-S_i^{hyd} = dG_i^{hyd}(T)/dT = 8.4 \pm 0.5$ for K^+ (bottom right with yellow circle), 20.8 ± 1.1 for Na^+ and 24.2 ± 0.9 for Cl^- (bottom left with green circle and blue diamond, respectively), 32.2 ± 1.5 for OH^- and 35.4 ± 2.0 for H_3O^+ (top right with red circle and blue triangle, respectively), and 30.8 ± 0.8 for TMA^+ and 72.4 ± 3.0 for TBA^+ (top left with black and red down triangles, respectively).

are from −59.3 to −68.9 kcal/mol, while experimental values are −70.5 and −71.2 kcal/mol.[38,39] Regarding Na^+, values are ranging between −76.5 and −91.6 kcal/mol, but experimental values are −87.2 and −88.7 kcal/mol.[38,39] With respect to Cl^-, calculated values range between −90.1 and −103.8 kcal/mol, and experimental values are −81.3 and −89.1 kcal/mol.[38,39] Note that there is a broad difference of around 8 kcal/mol in the two experimental data and all force field parameters for Cl^- present $G_i^{hyd}(298)$ closer to the highest experimental value. Concerning OH^- and H_3O^+, values are from −107.2 to −136.3 kcal/mol and from −103.4 to −110.5 kcal/mol, and experimental values are −105.0 and −110.4 kcal/mol,[40] respectively. The differences between the experimental and theoretical values of the hydration free energy, ΔG_i^{hyd}(exp/theor), at 298 K are shown in Figure 1 considering different experimental values, ionic force field parameters, and water models. It can be seen that the best agreement between experimental/theoretical values (less than 1.5 kcal/mol) is

https://doi.org/10.1021/acs.jctc.1c00116
J. Chem. Theory Comput. 2021, 17, 3539−3553

observed for the ionic force field parameters proposed by: Smith and Dang[45] for Cl^- and Na^+, Beglov and Roux[50] for K^+, and us (those proposed herein) for OH^- and H_3O^+. As a general trend, both water models present similar values for G_i^{hyd} but with the TIP3P model, the ΔG_i^{hyd}(exp/theor) values are slightly smaller than with SPC/E.

For all anions and cations, $G_i^{hyd}(T)$ becomes increasingly negative as temperature becomes lower, that is, $\Delta G_i^{hyd}/\Delta T > 0$. The $G_i^{hyd}(T)$ behavior with respect to temperature is better depicted in Figure 2 for ionic force field parameters that achieved the best experimental/theoretical agreement and the SPC/E water model. Regardless of ion charge, the dependence of $G_i^{hyd}(T)$ on temperature is linear, and all of which are better hydrated at lower temperatures, but the angular coefficient of the best linear fit is force field-dependent. As a general trend, it was observed that polyatomic ions (H_3O^+, OH^-, TBA^+, and TMA^+) are more sensitive to temperature variation, that is, $\Delta G_i^{hyd}/\Delta T$ is larger for polyatomic ions than for monoatomic ions (Cl^-, Na^+, and K^-).

By calculating G_i^{hyd}, two contributions can be obtained separately, which are the electrostatic and nonelectrostatic terms $G_i^{hyd} = G_{ele}^{hyd} + G_{non\text{-}ele}^{hyd}$. Changes in these two terms based on temperature are shown in the Supporting Information. It is known that the $G_{non\text{-}ele}^{hyd}$ term is composed by dispersion (always negative) and cavitation (always positive) contributions for the free energy. For all ions, the cavitation contribution is dominant, once it results in a positive $G_{non\text{-}ele}^{hyd}$. This term, in particular, has decreased sensitivity to temperature change and lower magnitude from 0.1 to 5.9 kcal/mol for monoatomic ions, 0.8 to 4.6 kcal/mol for aqueous ions, and 1.8 to 8.6 kcal/mol for alkyl ions by considering all force field parameters. For the latter two, $G_{non\text{-}ele}^{hyd}$ is proportional to the size of the chain, which is larger for TBA^+ than TMA^+. On the other hand, the term G_{ele}^{hyd} is negative for all ions. It has greater sensitivity to temperature change and it is larger in magnitude than $G_{non\text{-}ele}^{hyd}$, that is, from −64.8 to −107.2 kcal/mol for monoatomic ions, −103.5 to −139.9 kcal/mol for aqueous ions, and −22.1 to −39.8 kcal/mol for alkyl ions, again considering all force field parameters. Changes in $G_i^{hyd}(T)$ due to different temperatures arise predominantly from electrostatic interactions. G_{ele}^{hyd} increases as follows: $TBA^+ < TMA^+ < K^+ < Na^+ < Cl^- < OH^- < H_3O^+$ for force field parameters that reached the best experimental/theoretical agreement at room temperature.

The solvation distribution of water molecules around ions has been analyzed by the radial distribution function, $G(r)$, at different temperatures (Figures are shown in the Supporting Information). As expected, specific interactions between water molecules and monoatomic or aqueous ions can be easily identified at distances of around 0.2−0.3 nm comprising the first maximum of $G(r)$ between ions and the atoms of oxygen and hydrogen in water, that is, ion-OW and ion-HW. In the case of negative ions, the $G_{ion\text{-}HW}(r)$ peak is closer (around 0.1 nm) than the $G_{ion\text{-}OW}(r)$ peak, while the $G_{ion\text{-}OW}(r)$ peak is closer in the case of positive ions while describing hydrogen bond formation. However, in the case of alkyl ions, $G_{ion\text{-}OW}(r)$ and $G_{ion\text{-}HW}(r)$, peaks appear at the same position (around 0.4−0.5 nm) showing a tangential orientation of the OH bond of water molecules. Thus, no specific interactions with water molecules are found around TMA and TBA ions indicating clathrate formation. $G(r)$ presents very small differences with respect to temperature changes. Tables showing distances of the beginning, maximum, and first minimum of $G(r)$ and the coordination numbers of ions with temperature ranging from 293 to 353 K are shown in the Supporting Information. Differences that are smaller than 0.02 nm were observed for the first peak and the largest variation of the coordination number was found in a reduction of less than 1.6 water molecules (<10% of the first solvation shell) for TMA^+ and TBA^+ when temperature increased from 293 to 353 K. Therefore, it is concluded that the temperature effect in the range of 293−353 K is negligible in the solvation structure of water molecules around ions.

An increase in G_i^{hyd} for rising temperatures means that the cold side is preferred by ions diffusing in a temperature gradient. The difference $\Delta G_i^{hyd}(T) = G_i^{hyd}(T + \delta T) - G_i^{hyd}(T)$ in an initially homogeneous ionic solution with an instantaneously applied temperature gradient is due to the maximum probability density shift along time, as the ion moves toward the position of lower free energy. The success of using physical parameters obtained from the thermodynamic equilibrium for describing non-equilibrium effects has been discussed in the literature.[29,37] It is a probabilistic point of view that explains the reasons for increasing ion concentration in one side of a temperature gradient, in which Fick law of diffusion assumes a similar strength due to the induced concentration gradient. It is worth mentioning that the directional diffusion phenomena expressed by the Fick equation for diffusion with a drift term[53] modulates inhomogeneity in concentration induced by the temperature gradient. Therefore, the amount of possible ions that migrates toward the cold side is defined by the difference $\Delta G_i^{hyd}(T)$, but the time to stabilize concentration distribution depends on the self-diffusion constant, which is to be discussed as follows.

2.2. Ion and Salt Diffusion. The rate of ion displacement is related to the shift in the maximum probability density toward a position with lower free energy in a temperature gradient and is quantified by the self-diffusion coefficient, D_i.[37] By calculating the slope of the ionic MSD through MD simulations at different temperatures (the same temperatures shown in Table 1), values for $D_i(T)$ were obtained, which are shown in Table 2 for ionic force field parameters with the best experimental/theoretical agreement of $G_i^{hyd}(298)$. For comparison purposes, some experimental values[8,41] available in the literature are also presented. The values of $D_i(T)$ obtained from MD simulations

Table 2. Self-Diffusion Coefficients of Ions, $D_i(T)$ (in 10^{-5} cm^2/s), in Aqueous Solution Calculated Using MD Simulations at Different Temperatures Using Force Field Parameters with the Best Experimental/Theoretical Agreement (Dang for Cl^- and Na^+, Roux for K^+, and ours for OH^-, H_3O^+, TMA^+, and TBA^+) and the SPC/E Water Model[a]

ion	D_i(293)	D_i(298)	D_i(313)	D_i(333)	D_i(353)
Cl^-	1.45	2.12 [2.03][b]	2.55	3.06	3.48
K^+	1.27	1.89 [1.96][b]	2.17	3.11	4.19
Na^+	0.95	1.45 [1.33][b]	1.77	2.38	3.33
OH^-	[4.76][c]	2.17 [5.32][b]	[7.03][c]	[9.55][c]	[12.41][c]
H_3O^+	[8.50][c]	2.45 [9.31][b]	[11.72][c]	[14.99][c]	[18.22][c]
TMA^+	0.91	1.15 [1.20][b]	1.34	2.14	2.54
TBA^+	0.38	0.49 [0.51][b]	0.66	0.79	1.21

[a]Experimental values are in brackets. [b]Evaluated values taken from experimental measurements, ref 8. [c]Evaluated values taken from experimental measurements of ionic conductivity, ref 41. To convert ionic conductivity, $C_i(T)$, into ion self-diffusion $D_i(T)$, the Nernst−Einstein equation was used: $D_i(T) = RTC_i(T)/F^2$, where R is the ideal gas constant, T is the temperature, and F is the Faraday constant. The standard deviation of calculated $D_i(T)$ is lower than 0.10×10^{-5} cm^2/s.

https://doi.org/10.1021/acs.jctc.1c00116
J. Chem. Theory Comput. 2021, 17, 3539−3553

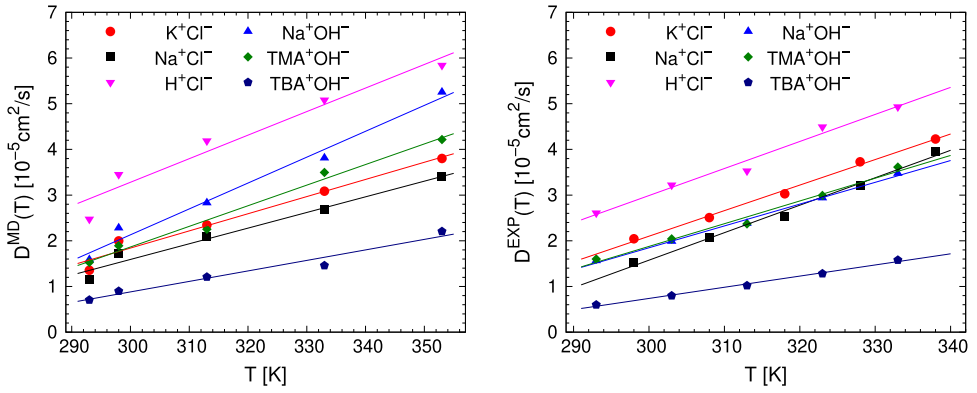

Figure 3. Effective mass diffusion $D(T)$ (in 10^{-5} cm^2/s) for different temperatures: (left) calculated $D^{MD}(T)$ using eq 3 with ion self-diffusion coefficients D_i shown in Table 2 and (right) experimental $D^{EXP}(T)$ obtained from optical experiments.[16,42] The symbols and colors represent different salts: K^+Cl^- (red circle), Na^+Cl^- (black square), H^+Cl^- (pink down triangle), Na^+OH^- (blue triangle), TMA^+OH^- (green diamond), and TMA^+OH^- (dark blue pentagon).

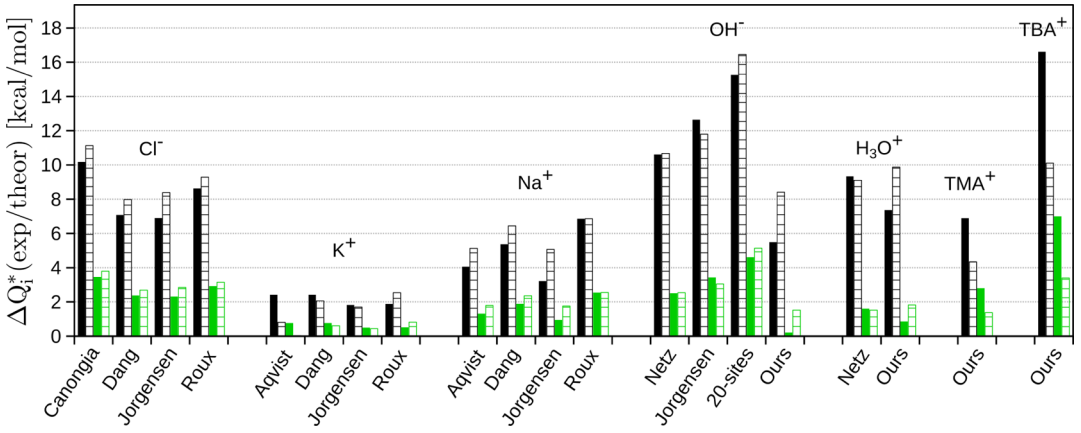

Figure 4. Experimental/theoretical differences of the single-ion heat of transport, ΔQ^*(exp/theor) at T = 298 K for different ionic force field parameters with two water models: SPC/E (solid bar) and TIP3P (open bar). The colors represent two theoretical procedures MD (black) and MD/TN (green) in comparison with the experimental data obtained by Agar et al.[8]

are in good agreement with experimental data with less than 0.09 $\times 10^{-5}$ cm^2/s of difference, except for hydroxide and hydronium ions whose calculated values are highly underestimated at room temperature (2.17 and 2.45 $\times 10^{-5}$ cm^2/s) for OH^- and H_3O^+, respectively, in comparison with 5.32 and 9.31 $\times 10^{-5}$ cm^2/s obtained experimentally. However, it is well-known in the literature that the diffusion of hydroxide and hydronium in aqueous solutions occurs predominantly by a Grotthus-type mechanism involving proton exchange between water molecules.[54] This mechanism is not considered in classical MD simulations because water molecules are not able to protonate/deprotonate in classical MD simulations. It requires more sophisticated methodologies, such as first-principles MD simulations, among other techniques.[55,56] Due to such a limitation of MD simulations, we decided to use the experimental values found in the literature[41] for OH^- and H_3O^+ at different temperatures (shown in Table 2) for further calculations in this work.

By increasing temperatures from 293 to 353 K, a diffusion coefficient increase between 2.1 times for the H_3O^+ ion and up to 3.5 times for the Na^+ ion was found. At room temperature, the calculated self-diffusion coefficient $D_i(298)$ shows that ions follow the same experimental tendency:[8] $TBA^+ < TMA^+ < Na^+ < K^+ < Cl^- < OH^- < H_3O^+$, in which the TBA^+ is the slowest ion and H_3O^+ is the fastest ion in aqueous solutions. An increase in D_i values from temperature differences is expected due to increased thermal energy and decreased water viscosity. Temperature gradients in aqueous electrolytes mean that the self-diffusion coefficient is position-dependent, that has been assigned as a source of thermophoretic migration in the temperature gradient.[57] This effect is, in principle, not related to the single-ion Soret effect.

Once the values of ion self-diffusion coefficients D_i (shown in Table 2) are obtained, the effective mass diffusion D of salts has been calculated for different temperatures using the following equation[7]

$$D = \frac{2D_+D_-}{D_+ + D_-} \tag{3}$$

The calculated values of $D(T)$ and experimental data[16,42] are shown in Figure 3. All values are presented in the Supporting Information. There is a good agreement between calculated and experimental values for all salts. The calculated values are in the range of 0.7 and 5.9 $\times 10^{-5}$ cm^2/s and experimental values range from 0.6 to 5.3 $\times 10^{-5}$ cm^2/s. The dependence of effective mass diffusion $D(T)$ on temperature for both sets of data presents a linear growth as temperature increases for all salts.

The smallest slope is 0.02 $\times 10^{-5}$ cm^2/sK obtained for TBA^+OH^- in both sets and the slopes of other salts (K^+Cl^-, Na^+Cl^-, H^+Cl^-, Na^+OH^-, and TMA^+OH^-) are between 0.05

https://doi.org/10.1021/acs.jctc.1c00116
J. Chem. Theory Comput. 2021, 17, 3539−3553

Table 3. Single-Ion Heat of Transport Q_i^* (in kcal/mol) Calculated at T = 298 K Using MD and MD/TN Approaches[a]

		Q_i^*			α_i			$j_{Ti}/c = \alpha_i D_i$		
Ion	force field	MD	MD/TN	agar	MD	MD/TN	agar	MD	MD/TN	agar
Cl^-	Canongia Lopes	10.31	3.59	[0.13]	8.71	3.03	0.11	18.46	6.42	0.23
	Dang	7.21	2.51		6.09	2.12		12.91	4.49	
	Jorgensen	7.03	2.45		5.94	2.07		12.59	4.38	
	Roux	8.76	3.05		7.40	2.57		15.68	5.46	
K^+	Åqvist	3.04	1.39	[0.62]	2.57	1.17	0.52	4.85	2.22	0.98
	Dang	3.04	1.39		2.57	1.17		4.85	2.22	
	Jorgensen	2.44	1.12		2.06	0.94		3.90	1.78	
	Roux	2.50	1.14		2.11	0.97		3.99	1.83	
Na^+	Åqvist	4.89	2.15	[0.83]	4.13	1.81	0.70	5.98	2.63	1.02
	Dang	6.20	2.72		5.23	2.30		7.59	3.33	
	Jorgensen	4.05	1.78		3.42	1.50		4.96	2.18	
	Roux	7.69	3.38		6.49	2.85		9.41	4.13	
OH^-	Netz	14.72	6.62	[4.11]	12.43	5.59	3.48	66.13	29.76	18.51
	Jorgensen	16.75	7.54		14.14	6.36		75.23	33.85	
	20-sites	19.37	8.72		16.35	7.36		87.01	39.15	
	ours	9.60	4.32		8.10	3.65		43.10	19.40	
H_3O^+	Netz	12.52	4.79	[3.18]	10.57	4.05	2.70	98.38	37.68	25.14
	ours	10.55	4.04		8.91	3.41		82.92	31.76	
TMA^+	ours	9.18	5.09	[2.39]	7.75	4.30	2.02	8.91	4.95	2.32
TBA^+	ours	21.58	11.97	[4.97]	18.22	10.11	4.21	8.93	4.95	2.06

[a]In brackets are the values obtained experimentally by Agar et al.,[8] Q_i^*(Agar). Single-ion Soret coefficient α_i (eq 2) and single-ion reduced mass current density j_{Ti}/c (eq 1) were calculated with three sets of Q_i^*.

and 0.06×10^{-5} cm^2/sK for experimental sets and between 0.03 and 0.06×10^{-5} cm^2/sK for calculated sets. The most pronounced difference was found in the D slope of Na^+Cl^-, 0.03×10^{-5} cm^2/sK for calculated values and 0.06×10^{-5} cm^2/sK for experimental data. All the linear regressions are presented in the Supporting Information. TBA^+OH^- has the lowest effective diffusion, H^+Cl^- has the highest effective diffusion, and the other salts have an intermediate diffusion. These behaviors reflect the values of ion self-diffusion coefficients D_i (see Table 2), where the TBA^+ ion has the smallest $D_i(298) = 0.51 \times 10^{-5}$ cm^2/s and the H_3O^+ ion has the largest $D_i(298) = 9.31 \times 10^{-5}$ cm^2/s.

2.3. Ion Thermodiffusion. The single-ion heat of transport Q_i^* and the single-ion Soret coefficient α_i were calculated from the dependence of the ion hydration free energy $G_i^{hyd}(T)$ on temperature. Then, using α_i and the ion self-diffusion coefficient $D_i(T)$, the ion mass current density j_{Ti} that describes the thermodiffusion of ions in aqueous solutions was calculated. In Figure 2, a linear dependence of $G_i^{hyd}(T)$ on temperature and a positive slope for all ions in the range of T = 293−353 K are shown. Therefore, the angular coefficient of the linear best fit of calculated $G_i^{hyd}(T)$ is constant and positive in this temperature range and was used to calculate the modules of $S_i^{hyd}(T)$. Furthermore, the value of modules of the single-ion heat of transport Q_i^* was obtained using two approaches: (i) the direct calculation from the MD simulation, $Q_i^*(MD) = -TS_i^{hyd}$; and (ii) the scaling factor of Takeyama and Nakashima,[31] $Q_i^*(MD/TN) = -f_i^{TN}TS_i^{hyd}$ where the scaling factor f_i^{TN} is 0.348 for Cl^-, 0.383 for OH^-, 0.439 for Na^+, 0.450 for H_3O^+, 0.457 for K^+, and 0.555 for TMA^+ and TBA^+.

In Figure 4, we compared these two sets of calculated values, $Q_i^*(MD)$ and $Q_i^*(MD/TN)$, for different ionic force field parameters and two water models (SPC/E and TIP3P) with the experimental values obtained by Agar et al.,[8] Q_i^*(Agar). The best agreement between experimental/theoretical values, $\Delta Q_i^*(exp/theor)$, was observed for the MD/TN procedure (green bars) showing that the scaling factor f_i^{TN} improves the calculated values of $Q_i^*(MD/TN)$ in comparison with Q_i^*(Agar). As a general trend, both water models (solid bars for SCP/E and open bars for TIP3P) present similar values, but with the SPC/E model, the $\Delta Q_i^*(exp/theor)$ values are slightly smaller than with TIP3P. Therefore, for further discussions, we will present only the results obtained with the SPC/E water model (the results for TIP3P are shown in the Supporting Information), but it is important to note that all conclusions are valid for both water models. Another interesting observation concerning Q_i^* is that there is a good performance of the same force field parameters that reached the best experimental/theoretical agreement for $G_i^{hyd}(T)$: Dang for Cl^- and Na^+, Roux for K^+, and ours for OH^-, H_3O^+, TMA^+, and TBA^+. They present $\Delta Q_i^*(exp/theor) < 2.5$ kcal/mol, except for TBA^+ with $\Delta Q_i^*(exp/theor) > 3.5$ kcal/mol. However, Jorgensen force field parameters for monoatomic ions present a slightly better performance in comparison due to the better temperature dependence of $G_i^{hyd}(T)$ for Cl^-, Na^+, and K^+.

Table 3 shows the experimental data,[8] Q_i^*(Agar), and the two sets of theoretical values, $Q_i^*(MD)$ and $Q_i^*(MD/TN)$, obtained by MD simulations with different ionic force field parameters and the SPC/E water model at T = 298 K. The values obtained with the TIP3P water model are shown in the Supporting Information.

Using eq 2, we obtained the corresponding sets of single-ion Soret coefficient α_i values: $\alpha_i(MD)$, $\alpha_i(MD/TN)$, and α_i(Agar). By comparing Q_i^* and α_i shown in Table 3, it is possible to observe that the three sets of values present a similar trend: the values for polyatomic ions are higher than those for monoatomic ions. The values of Q_i^*(Agar) and α_i(Agar) increase as follows $Cl^- < K^+ < Na^+ < TMA^+ < H_3O^+ < OH^- < TBA^+$.

As for OH^- and H_3O^+, the best calculated values for $\alpha_i(MD/TN)$ are 3.65 and 3.41 which are in very good agreement with α_i(Agar) values, 3.48 and 2.70, respectively, using our force field parameters. Regarding K^+, Na^+, TMA^+, and TBA^+, the best

https://doi.org/10.1021/acs.jctc.1c00116
J. Chem. Theory Comput. 2021, 17, 3539−3553

calculated values for α_i(MD/TN) are 0.94, 1.50, 4.30, and 10.11 that are around two times larger than α_i(Agar) values, 0.52, 0.70, 2.02, and 4.21, respectively, using Jorgensen force field parameters for monoatomic ions and our parameters for polyatomic ions. Cl^- is the only ion in which the best calculated value, α_{Cl^-}(MD/TN) = 2.07, is far from α_{Cl^-}(Agar) = 0.11 by a factor of 20 times. Therefore, we believe that new force field parameters for Cl^- should be developed in the future to better describe the heat of transport and Soret coefficient. The current force field parameters are able to reproduce the hydration free energy of Cl^- (the highest experimental value) and self-diffusion coefficient, as shown in Tables 1 and 2, respectively. However, they fail to describe its derivative with respect to temperature, $\Delta G_i^{hyd}(T)/\Delta T$.

Our results show that the presence of temperature gradient in salted water induces an increasing ion concentration toward the cold side of the solution for all studied cations and anions due to the hydration free energy $G_i^{hyd}(T)$ temperature dependence. Therefore, the single-ion Soret coefficient α_i together with the rate of ion displacement described by the self-diffusion coefficient D_i generates different intensities of ion flux given by eq 1. Assuming that an experimental setup can be prepared using the same values of the numerical volumetric concentration of ions n_i and temperature gradient ∇T for all ions, we analyzed the reduced mass current density $j_{Ti}/c = \alpha_i D_i$, where $c = -n_i \nabla T/T$. The calculated values of j_{Ti}/c at room temperature are shown in Table 3. The values of ion flux intensity j_{Ti}/c(Agar) increase as follows $Cl^- < K^+ < Na^+ < TBA^+ < TMA^+ < OH^- < H_3O^+$. Then, by comparing this sequence with the α_i(Agar) sequence ($Cl^- < K^+ < Na^+ < TMA^+ < H_3O^+ < OH^- < TBA^+$) and D_i sequence ($TBA^+ < TMA^+ < Na^+ < K^+ < Cl^- < OH^- < H_3O^+$), it is possible to conclude that the flux of monoatomic ions is dominated by single-ion Soret coefficients, while the flux of polyatomic ions is dominated by self-diffusion coefficients. This information is important, since it can be used to plan ion combination that may generate salts with a better thermodiffusion effect.

2.4. Thermodiffusion of Salts. In a thermodiffusion analysis, the stationary state of the concentration gradient is considered, that is, the total ionic flux is null. Then, $j_T + j_n = 0$, where $j_T = -nD_T\nabla T$, $j_n = -D\nabla n$, D_T is the salt thermal diffusion coefficient, and D is the effective mass diffusion coefficient. In the case where positive and negative ions are not distinguished, the salt Soret coefficient is simply defined as $S_T = D_T/D$. The values of S_T and D are experimentally accessible from amplitudes and transients, respectively, of optical experiments[16,42] in which the probe volume of samples are infinitely larger in comparison with ionic sizes. However, by distinguishing anions (α_- and D_-) and cations (α_+ and D_+), the stationary state has additional relations,[7] such as

$$S_T = \frac{\alpha_+ + \alpha_-}{T} \tag{4}$$

and eq 3. As both descriptions should be equivalent, it is possible to find the following relation

$$D_T = \frac{D(\alpha_+ + \alpha_-)}{T} \tag{5}$$

therefore, using eqs 4 and 5, we calculate the salt Soret coefficient S_T and the salt thermal diffusion coefficient D_T, respectively. In addition, we performed a discussion about their temperature dependence and a comparison with experimental values obtained with optical measurements.[16,42]

Figure 5 shows the salt Soret coefficient S_T calculated using single-ion Soret coefficients α_i (Table 3) at T = 298 K in comparison with experimental data.[16,42] The values are presented in Table 4 for force field parameters with the best experimental/theoretical agreement. As expected, the values of S_T obtained from $\alpha_i^*(Agar)$ are closer to experimental results, since they were calculated from $Q_i^*(Agar)$ obtained through calorimetric experiments assuming a infinite dilution,[8] except for the TBA^+OH^- salt where the experimental value S_T(Exp) = 5.40 × 10^{-2} 1/K is almost twice the S_T(Agar) = 2.60 × 10^{-2} 1/K. The calculated values for S_T obtained through MD simulations using different force field parameters for ions are indicated as intervals (horizontal bars) in Figure 5 and all individual values are shown in the Supporting Information. The two sets of calculated S_T, with MD and MD/TN, are in the same order of magnitude as the experimental data, but the approach MD/TN provides values closer to the experimental data. Both sets present a similar trend if compared to the experimental data: the values for salts composed of polyatomic ions (OH^-, H_3O^+, TMA^+, and TBA^+) are larger than those for salts composed of monoatomic ions (Cl^-, K^+, and Na^+). It can be seen that the scaling factor f_i^{TN} that relates the single-ion heat of transport to the ion hydration entropy proposed by Takeyama and Nakashima[31] improves the calculated values of the salt Soret coefficient, S_T(MD/TN), in comparison with experimental data, S_T(Exp). Analyzing the correlation between calculated and experimental values of S_T presented in Table 4, a linear regression of S_T(Exp) = 1.55 S_T(MD/TN) - 2.04 with R^2 = 96% was obtained, hence showing a very good correlation between both sets of data. An interesting additional observation is that the overestimated value of calculated α_{Cl^-}(MD/TN) imposes larger calculated values of S_T for chloride salts (K^+Cl^-, Na^+Cl^-, and H^+Cl^-), once S_T is proportional to $\alpha_+ + \alpha_-$. Thus, a better parametrization of the Cl^- force field can improve the agreement of calculated S_T(MD/TN) values with the experimental data even further. This

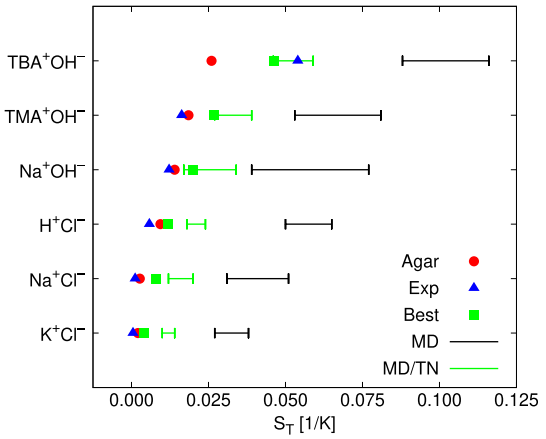

Figure 5. Salt Soret coefficient S_T (in 1/K) calculated using eq 4 with the single-ion Soret coefficient α_i shown in Table 3 and experimental data obtained by optical measurements.[16,42] The colors represent: S_T(Agar) (red), S_T(MD) (black), S_T(MD/TN) (green), and S_T(Exp) (blue). The horizontal bars represent the range obtained using MD simulations with different ionic force field parameters and the SPC/E water model. The green square with legend "Best" represents S_T(MD/TN) values calculated using the force field parameters with the best experimental/theoretical agreement (Dang for Cl^- and Na^+, Roux for K^+, and ours for OH^-, H_3O^+, TMA^+, and TBA^+) and the SPC/E water model but with the modified Cl^- Soret coefficient, $\alpha_{Cl^-}^{Best} = \alpha_{Cl^-}/10$.

https://doi.org/10.1021/acs.jctc.1c00116
J. Chem. Theory Comput. 2021, 17, 3539−3553

Table 4. Salt Soret Coefficient S_T (in $\times 10^{-2}$ 1/K) Shown in Figure 5 and Fast and Slow Seebeck Coefficients, S_{fast} and S_{slow} (in mV/K), Shown in Figure 7[a]

	S_T			S_{fast}			S_{slow}		
Salt	MD/TN	agar	Exp[42]	MD/TN	agar	Exp[43]	MD/TN	Agar	Exp[43]
K^+Cl^-	1.04	0.21	0.05	0.10	0.04	0.30	0.10	0.01	0.17
	(0.40)			(0.06)			(0.07)		
Na^+Cl^-	1.48	0.27	0.12	0.06	0.03	0.50	0.02	0.03	1.60
	(0.80)			(0.13)			(0.18)		
H^+Cl^-	1.86	0.94	0.58	0.42	0.46	0.90	0.11	1.10	2.00
	(1.20)			(0.48)			(0.28)		
Na^+OH^-	1.99	1.40	1.22	0.42	0.43	0.30	0.12	1.30	1.10
TMA^+OH^-	2.67	1.85	1.63	0.38	0.38	0.50	0.06	0.83	1.20
TBA^+OH^-	4.62	2.60	5.40	0.42	0.48	0.20	0.56	2.10	3.60

[a]MD/TN values were obtained using ionic force field parameters with the best experimental/theoretical agreement (Dang for Cl^- and Na^+, Roux for K^+, and ours for OH^-, H_3O^+, TMA^+, and TBA^+) and the SPC/E water model. In parentheses are values calculated using $\alpha_{Cl^-}{}^{Best}$.

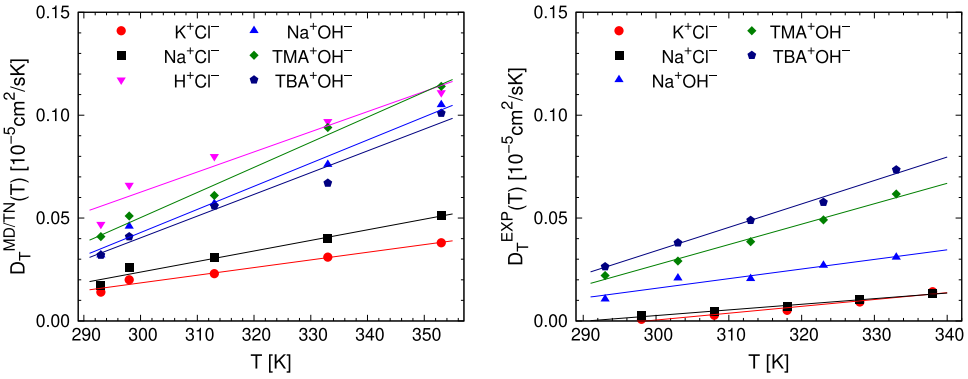

Figure 6. Thermodiffusion coefficient $D_T(T)$ (in 10^{-5} cm^2/sK) for different temperatures: (left) calculated $D_T^{MD/TN}(T)$ using eq 5 with single-ion Soret coefficients α_i(MD/TN) shown in Table 3 and effective mass diffusion $D(T)$ shown in Figure 3 and (right) experimental $D_T^{EXP}(T)$ obtained from optical experiments.[16,42] The symbols and colors represent different salts: K^+Cl^- (red circle), Na^+Cl^- (black square), H^+Cl^- (pink down triangle), Na^+OH^- (blue triangle), TMA^+OH^- (green diamond), and TMA^+OH^- (dark blue pentagon).

hypothesis was assessed by dividing the α_{Cl^-}(MD/TN) by a factor of 10, that is, $\alpha_{Cl^-}{}^{Best} = \alpha_{Cl^-}/10$, and recalculating the S_T for chloride salts shown in Figure 5 and in parentheses in Table 4.

A broadly discussed topic in thermodiffusion is the temperature dependence of the salt Soret coefficient S_T and the salt thermal diffusion coefficient D_T.[18,19,23−25,33,35,42] Using the relation between D_T and α_i (eq 5), the temperature dependence of the salt thermal diffusion coefficient $D_T(T)$ was analyzed. Note that the calculated single-ion Soret coefficients α_i for all salts were obtained as a constant and positive at temperatures ranging from 293 to 353 K. Then, we used the calculated effective mass diffusion coefficient D (shown in Figure 3) obtained for different temperatures to calculate $D_T(T)$. These results of $D_T(T)$ calculated through α_i(MD/TN) are shown in Figure 6 together with the experimental data[16,42] for comparison purposes. All values are presented in the Supporting Information. There was a good agreement between the calculated and experimental values for all salts. The best agreement is for TBA^+OH^- where the calculated values are in the range of 0.032 to 0.067 $\times 10^{-5}$ cm^2/sK at temperatures from 293 to 333 K, and experimental values are in the range of 0.026 to 0.074 $\times 10^{-5}$ cm^2/sK for the same temperature range. The linear temperature dependence seen for calculated $D_T^{MD/TN}(T)$ resembles the linear dependence found in the experimental data. The slope of $D_T^{MD/TN}(T)$ ranges from 0.38 to 1.21 $\times 10^{-8}$cm^2/sK and $D_T^{EXP}(T)$ ranges from 0.27 to 1.14 $\times 10^{-8}$cm^2/sK, in which K^+Cl^- and Na^+Cl^- have the lowest values [$\sim 0.45 \times 10^{-8}$cm^2/sK for $D_T^{MD/TN}(T)$ and $\sim 0.30 \times 10^{-8}$cm^2/sK for $D_T^{EXP}(T)$] and TMA^+OH^- and TBA^+OH^- achieved the highest values [$\sim 1.10 \times 10^{-8}$cm^2/sK for $D_T^{MD/TN}(T)$ and $\sim 1.05 \times 10^{-8}$cm^2/sK for $D_T^{EXP}(T)$]. This analysis reveals that the temperature dependence of the thermodiffusion coefficient $D_T(T)$ is just a consequence of the temperature dependence of the ratio $D(T)/T$.

Different values of the single-ion Soret coefficients α_i for anions and cations mean that one kind of ion has a trend to flow more than the other one in temperature gradients. To avoid charge separation, a thermoelectric field arises in solution. This is usually described in a phenomenological way as the generalized equations for ion current density[7]

$$j_i = -D_i n_i \left(\frac{\partial \ln n_i}{\partial x} - \frac{z_i e}{k_B T} E_x + 2\alpha_i \frac{\partial \ln T}{\partial x} \right) \quad (6)$$

where z_i is the valence number, x is a space coordinate, and E_x is the hypothetical ad hoc thermoelectric field. Recently, it was shown that E_x arises from two dynamical effects that are distant in at least eight orders of magnitude in their transient times:[22] E_1 proportional to the difference of products $\alpha_+D_+ - \alpha_-D_-$, which affect the fast response of the system that is much longer than the Debye transient and much shorter than the diffusive transient, and E_2 is proportional to the difference $\alpha_+ - \alpha_-$, which affects the slow response of the system that is much longer than the diffusive transient.[22] The equations for amplitude modules of Seebeck coefficients related to both time transients are given by[22,58]

https://doi.org/10.1021/acs.jctc.1c00116
J. Chem. Theory Comput. 2021, 17, 3539−3553

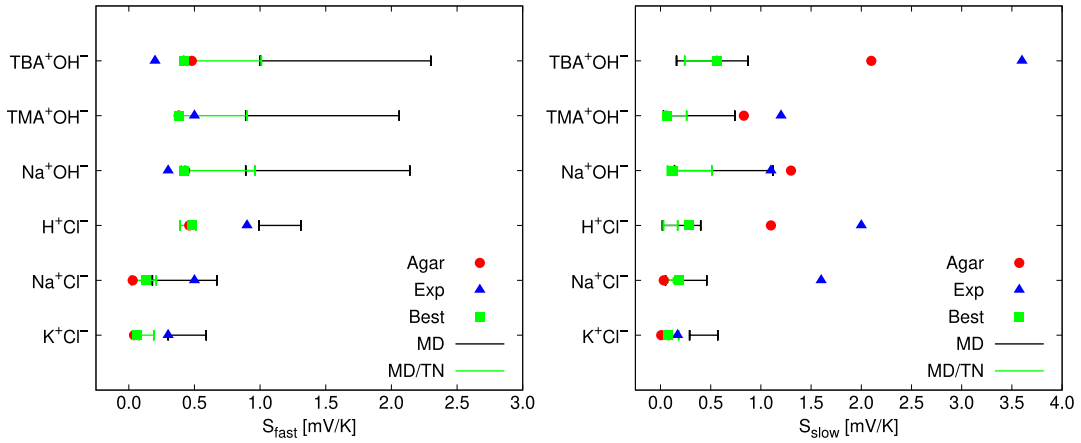

Figure 7. Modules of fast and slow Seebeck coefficients, S_{fast} (left) and S_{slow} (right) (in mV/K), calculated using eqs 7 and 8, respectively, with self-diffusion coefficients D_i shown in Table 2 and single-ion Soret coefficient α_i shown in Table 3, and the experimental data obtained with optical measurements.[43] The color and symbol descriptions are the same as shown in Figure 5.

$$S_{fast} = \frac{2k_B}{e}\left|\frac{\alpha_+ D_+ - \alpha_- D_-}{D_+ + D_-}\right| \quad (7)$$

and

$$S_{slow} = \frac{k_B}{e}|\alpha_+ - \alpha_-| \quad (8)$$

In Figure 7, we show the calculated modules of fast and slow Seebeck coefficients, S_{fast} and S_{slow}, using eqs 7 and 8 with the self-diffusion coefficient D_i and single-ion Soret coefficients α_i showed in Tables 2 and 3, respectively. All values of different force field parameters for ions and water molecules are presented in the Supporting Information. Table 4 presents the values obtained using MD/TN approximation for simulations with force field parameters with the best experimental/theoretical agreement and the SPC/E water model. All values for the other force field are presented in the Supporting Information. The calculated values for S_{fast} obtained from the single-ion Soret coefficient α_i(MD/TN) and α_i(Agar) are close to the experimental data.[43] S_{fast}(MD/TN) values are in the range of 0.06 to 0.42 × 10^{-2} 1/K and experimental values are in the range of 0.2 to 0.9 × 10^{-2} 1/K.

A comparison between calculated and experimental values is shown in Figure 7(*left*). We found a large correlation between S_{fast}(MD/TN) and S_{fast}(Agar) with R^2 = 96%, which shows that the self-diffusion of anions and cations, D_- and D_+, dominates the fast response of the thermoelectric field, since S_{fast}(MD/TN) and S_{fast}(Agar) were calculated using the same set of D_i values shown in Table 2. No correlation between S_{fast}(MD/TN), or S_{fast}(Agar), and the experimental data was observed, R^2 < 10%. It means that although the values predicted by the DM/TN approach and the single-ion heat of transport Q_i^* experimentally determined by Agar et al.[8] are in the same order of magnitude as the experimental data, they cannot predict the fast thermoelectric response. Nevertheless, in general, there is still a lack of experimental results for the fast thermoelectric field of salts in aqueous solutions so as to establish definite conclusions.

On the other hand, a theoretical prediction using calculated values of S_{slow} is more important, since it describes the system after reaching the thermoelectric equilibrium long after the ionic diffusion has taken place. A comparison between calculated and experimental values is shown in Figure 7(*right*). Attention ought to be given to the order of magnitude for calculated Seebeck coefficients, as it is the same as the one obtained from experiments involving aqueous electrolytes.[1,2,59] S_{slow}(MD/TN) values are in the range of 0.02 to 0.56 mV/K and experimental values are in the range of 0.17−3.60 mV/K. Therefore, S_{slow}(MD/TN) presents lower values than the S_{slow}(Exp). However, we found a linear correlation between S_{slow}(MD/TN) and S_{slow}(Exp) with R^2 = 66% which has been improved when $\alpha_{Cl^-}^{Best}$ was used, R^2 = 90%. Figure 8 shows this last correlation with R^2 = 90% between S_{slow}(MD/TN) using $\alpha_{Cl^-}^{Best}$ and S_{slow}(Exp) and additionally the correlation between S_{slow}(Agar) and S_{slow}(Exp) with R^2 = 61%. For S_{slow}(Agar), it can be seen that the values for Na^+Cl^- (open red triangle) and Na^+OH^- (solid red triangle) present large deviation with respect to the linear fit (dashed red line) causing a weak correlation between them, but its slope is near 1.0 showing values of

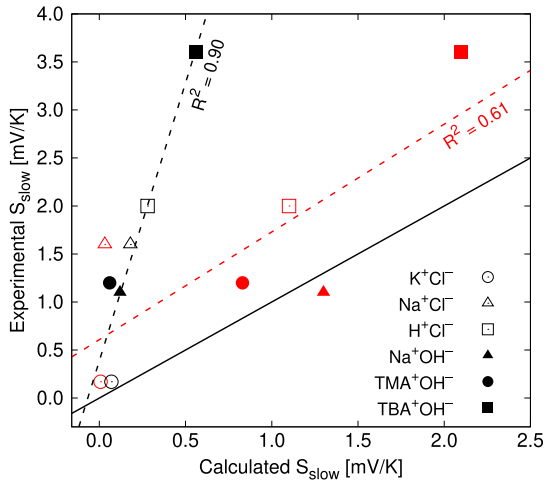

Figure 8. Relation between calculated and experimental modules of the slow Seebeck coefficient (in mV/K): S_{slow}(MD/TN) (black symbols) and S_{slow}(Agar) (red symbols) shown in Table 4. The symbols represent different salts: K^+Cl^- (open circle), Na^+Cl^- (open triangle), H^+Cl^- (open square), Na^+OH^- (solid triangle), TMA^+OH^- (solid circle), and TMA^+OH^- (solid square). The dashed lines represent the linear relation of S_{slow}(Exp) = 5.79 S_{slow}(MD/TN) + 0.39 with R^2 = 90% (black) and S_{slow}(Exp) = 1.12 S_{slow}(Agar) + 0.61 with R^2 = 61% (red). The solid black line represents a complete agreement between calculated and experimental values.

https://doi.org/10.1021/acs.jctc.1c00116
J. Chem. Theory Comput. 2021, 17, 3539−3553

S_{slow}(Agar) close to the experimental data S_{slow}(Exp), as shown in Table 4. On the other hand, for S_{slow}(MD/TN), all calculated values (black symbols) are close to the linear fit (dashed black line) given a strong correlation between experimental/theoretical values. Therefore, the theoretical MD/TN procedure can predict the experimental values of the Seebeck coefficient through the following relation: $S_{slow}(Exp) = 5.79\ S_{slow}(MD/TN) + 0.39$.

The theoretical approach proposed herein using MD simulations and the scaling factor f_i^{TN} between the hydration entropy for ions S_i^{hyd} and the single-ion heat of transport Q_i^* is capable of predicting the Seebeck coefficient and describing the thermodiffusion of salts in aqueous solutions. We suggest that this approach is suitable to be used in the description of experimental results, such as those obtained by Zhao et al.[9] and Li et al.,[2] who had performed experimental measurements of aqueous electrolytes with optimized interfaces or porous-confining media to generate strong, unpredictable, and unprecedented Seebeck coefficients. As recently remarked by Zhao et al.,[9] a good strategy to obtain a high thermoelectric response is to use electrolytes with a high self-diffusion difference between constituents.[1,3,60] A further step is to confirm that the high values of $\Delta D = D_+ - D_-$ are only partly responsible for the high Seebeck coefficient values. The results lead us to state that a fundamental condition is a strong variation of ionic hydration free energy $G_i^{hyd}(T)$ for dispersed solute (such as salts and polyelectrolytes) in water solution. In other words, high values of $\Delta\alpha = \alpha_+ - \alpha_-$ or/and $\Delta(\alpha_i D_i) = \alpha_+ D_+ - \alpha_- D_-$ render high values of the Seebeck coefficient S, mainly due to the slow thermodiffusion effect. Thus, our method can be used to theoretically verify the feasibility of new materials to be inserted into ionic solutions so as to present high Soret or Seebeck coefficients, that is, before carrying out time-consuming tests in the laboratory.

3. CONCLUSIONS

An analysis of the ionic hydration free-energy temperature dependence $G_i^{hyd}(T)$ obtained from MD simulations in water solution resulted in a temperature-constant ionic hydration entropy S_i^{hyd}, ionic heat of transport Q_i, and single-ion Soret coefficients α_i, which show a trend of good agreement with experimental results. All studied anions and cations prefer the cold side of the temperature gradient, that is, they have a positive single-ion Soret coefficient. Polyatomic ions, such as OH^-, H_3O^+, TBA^+, and TMA^+, present greater temperature dependence, thus resulting in a higher single-ion Soret coefficient α_i, while monoatomic ions, such as Na^+, K^+, and Cl^-, present lower temperature dependence due to achieving decreased α_i. Moreover, our analysis has revealed that most contributions for the temperature dependence of $G_i^{hyd}(T)$ are from the electrostatic ion−water interaction. However, for alkyl ions (TBA^+ and TMA^+), the nonelectrostatic ion−water interaction, that is, the van der Waals or Lennard−Jones (LJ) interaction, plays an important role at around 40% of $G_i^{hyd}(T)$ variation. By comparing our results to the experimental data, it was found that a better agreement was obtained using the scaling factor f_i^{TN} between the single-ion heat of transport Q_i^* and the ionic hydration entropy S_i^{hyd} proposed by Takeyama and Nakashima[31] (f_i^{TN} = 0.348 for Cl^-, 0.383 for OH^-, 0.439 for Na^+, 0.450 for H_3O^+, 0.457 for K^+, and 0.555 for TMA^+ and TBA^+). The calculated values of ion flux intensity $j_{Ti}/c = \alpha_i D_i$ increase as follows $Cl^- < K^+ < Na^+ < TBA^+ < TMA^+ < OH^- < H_3O^+$, where the flux of monoatomic ions is dominated by single-ion Soret coefficients α_i, while the flux of polyatomic ions is dominated by self-diffusion coefficients D_i.

From the calculated temperature-independent single-ion Soret coefficient α_i, the salt Soret S_T and fast and slow Seebeck, S_{fast} and S_{slow}, coefficients were calculated, which also show good agreement with experimental results. We discuss the specific topic of thermodiffusion, that is, the ionic temperature dependence on the thermal diffusion coefficient $D_T(T)$, which shows that $D_T(T)$ depends on the ratio $D(T)/T$, where $D(T)$ is the salt effective mass diffusion coefficient.

The simulation reported in this work was performed at infinite ionic dilutions, that is, adding more water molecules to the simulated box did not change the final result for $G_i^{hyd}(T)$. We proposed a consistent approach that allowed comparison with experiments, taking advantage of the existing connection between the equilibrium hydration free energy G_i^{hyd} and the nonequilibrium effect. A comparison between experimental data and results obtained with nonequilibrium MD simulations with a temperature gradient along the simulation box is not straightforward. Given the fact that MD simulations use thermostatic methods, most of which were formulated to describe the stage of temperature equilibrium and they have no realistic physical behavior in the nonequilibrium stage. Then, these thermostatic methods provide an unrealistic ionic flux through the temperature gradient.

In our point of view, the limitations of the theoretical approach proposed in this work to calculate thermodiffusion coefficients are the inherent limitations of classical molecular simulations that are related to a good parameterization of ions in order to adequately describe the temperature dependence of the hydration, or solvation, free energy and the impossibility to describe the self-diffusion of hydroxide and hydronium in aqueous solutions occurs predominantly by a Grotthus-type mechanism involving proton exchange between water molecules. However, this last limitation was avoided using the experimental values of the hydroxide and hydronium self-diffusion coefficients at different temperatures. Our theoretical approach may be used to estimate $G_i^{hyd}(T)$ of thermoelectric materials and predict the slow Seebeck responses, in addition to an intuitive use of materials with a large difference in self-diffusion and single-ion Soret coefficients obtained from pure electrolyte aqueous solutions. The possibility to perform MD simulations with large ionic concentration and connect the results with transport coefficients is desired for applications in thermoelectric devices and biological systems, usually those dispersed in ionic aqueous solutions.

4. METHODOLOGY

We have performed two types of MD simulations using the GROMACS package:[61] (i) the conventional dynamics (cMD) with the Newton equation of motion coupled with a stochastic thermostat to generate the ion−water trajectories, analyze the solvation shells around ions, and calculate the ion self-diffusion coefficient; and (ii) the stochastic dynamics (sMD) with the Langevin equation of motion with a small friction constant to calculate ion hydration free energy. These two methods are equivalent,[61,62] but sMD becomes more advantageous in the calculation of the free-energy variations due to the enhanced conformational search ability.[62] In both types, the simulated system was composed of an ion (Na^+, K^+, Cl^-, OH^-, H_3O^+, TMA^+, or TBA^+), a counterion (Na^+ or Cl^-) surrounded by 1000 (or 2000) water molecules in a cubic box (for the case of organic ions TMA^+ and TBA^+). The simulations were

https://doi.org/10.1021/acs.jctc.1c00116
J. Chem. Theory Comput. 2021, 17, 3539−3553

performed in an *NPT* ensemble at P = 1 atm at different temperatures in the range of 293−353 K. The *NPT* ensemble was obtained using a velocity eescaling thermostat[63] for temperature control in cMD simulations with a coupling constant of 0.1 ps and a Berendsen barostat[64] for pressure control with a coupling constant of 2 ps. In sMD, the temperature control is obtained directly from the Langevin equation of motion with a friction constant of 1.0 ps^{-1}. All interactions were computed inside a cutoff radius of 14 Å. A long-range correction for electrostatic interactions was treated with the smooth particle-mesh Ewald method[65] with cubic interpolation and a Fourier spacing of 14 Å. The equations of motion were integrated using the leapfrog algorithm[66] in cMD simulations and its stochastic version[67] in sMD simulations and implemented as an sd integrator in the GROMACS package.[68] In both types of simulations, a time step of 1 fs with constraints in all H bonds using the LINCS algorithm was used.[69] The center of mass motion was linearly removed for the whole system at each 200 fs. For cMD simulations, the thermalization stage was performed for 5 ns and the equilibrium stage was performed for 10 ns.

In order to obtain the ionic hydration free energy G_i^{hyd}, nonbonding interaction energies between the ion and the solvent were multiplied by a λ scaling factor ($0 < \lambda < 1$), where $\lambda = 0$ means totally turned-off interactions and $\lambda = 1$ means totally turned-on interactions. Therefore, the solvation process was performed in two stages: first, we used a set of 11 λ_{LJ} values with $\lambda_q = 0$ to create the LJ particle−water interaction and then with $\lambda_{LJ} = 1$, we used a set of 11 λ_q values to create the ion−water Coulomb interaction in the pre-existent LJ particle. The set of 11 values used for λ_{LJ} and λ_q are {0.0, 0.1, 0.2, 0.3, 0.4, 0.5, 0.6, 0.7, 0.8, 0.9, and 1.0}. To avoid problems in the initial configuration, for each simulation with λ_{LJ} and λ_q, we started with a thermalized configuration obtained from a previous cMD simulation with $\lambda_{LJ} = 1$ and $\lambda_q = 1$, and then, the thermalization stage was performed for 1 ns and the equilibrium stage was performed for 2 ns for sMD simulations. Therefore, in order to calculate the differences of hydration free energy $G_{\lambda i}^{hyd}$, the potential energy differences between each sMD simulation with neighboring λ were obtained through the BAR method[70] using the *gmx bar* command available in the GROMACS package. The sum of free-energy differences between each λ state for the LJ potential gives the nonelectrostatic contribution ΔG_{nele} to the hydration free energy and the Coulomb potential gives the electrostatic contribution ΔG_{ele}. By adding these two contributions, nonelectrostatic and electrostatic, the total ionic hydration free energy, $G^{hyd} = \Delta G_{nele} + \Delta G_{ele}$, is obtained.

The temperature dependence of hydration free energy $G_i^{hyd}(T)$ of each ion was investigated for several force field parameters (as described below) and 13 temperatures ranging between 293 and 353 K temperatures in the range of 5 K. From the linear best fitting of $G_i^{hyd}(T)$ for each ion, we obtained the hydration entropy, that is, the rate of change in G_i^{hyd} with temperature, $S_i^{hyd} = -dG_i^{hyd}/dT$. These results were used to calculate ionic thermodiffusive properties. In this context, we also tested the proportionality factor proposed by Takeyama and Nakashima[31] between the single-ion heat of transport and the ionic hydration entropy in water, $Q_i^*(MD/TN) = -f_i^{TN} T S_i^{hyd}(T)$ where the scaling factor f_i^{TN} is 0.348 for Cl^-, 0.383 for OH^-, 0.439 for Na^+, 0.450 for H_3O^+, 0.457 for K^+, and 0.555 for TMA^+ and TBA^+.

Self-diffusion coefficients D_i were calculated using Einstein relation between the MSD[71] of the ion and its self-diffusion coefficient D_i using the *gmx msd* command available in the GROMACS package. We obtained the MSD of the ion center of mass at five temperatures (293, 298, 313, 333, and 353 K) in the equilibrium stage of cMD simulations and using 50 thousand configurations separated by 200 fs in a trajectory of 10 ns. By the linear best fitting of the MSD curve in its linear regime, around 0 and 3 ns, we calculated the ion diffusion coefficient D_i.

The force field parameters adopted in the MD simulations were for water, the SPC/E model[72] and TIP3P model[73] and the traditional models available in the literature for Na^+, K^+, and Cl^-, which we will be referred to as: Åqvist,[48] Dang,[45,49] Jorgensen,[46] Roux,[47,50] and Canongia Lopes[44] (the latter was used only for Cl^-). For TMA^+ and TBA^+, we adopted the OPLS-AA force field[74,75] for LJ potential parameters (ε and σ for *C*, *H*, and *N*) and bonded potential parameters (bond distances, bonds angles, and dihedral angles); for Coulomb potential, atomic charges were calculated using the CHELPG procedure[76] to fit the electrostatic potential calculated with quantum mechanics (QM) in an optimized geometry of the ions, including the solvent polarization with the polarized continuum model (PCM).[77] The QM calculations were performed using the MP2 theory[78] and the basis set cc-pVDZ.[79] This procedure has been applied successfully in previous works.[80−82] For H_3O^-, we employed the model proposed by Netz.[51] For OH^-, we employed the models: Netz,[51] 20-sites,[52] and Jorgensen.[74] Furthermore, for H_3O^- and OH^-, we also used a new set of force field parameters proposed by us to better describe their hydration free energies at room temperature. For both ions, we obtained their QM optimized geometries at the MP2/aug-cc-pVQZ[79] level and the CHELPG atomic charges (only for hydroxide) at the MP4(SDQ)[83] /aug-cc-pVQZ level in water solution with solvent polarization included with the PCM model. For OH^-, we adopted the LJ parameters (ε and σ) of the UFF force field[84] but by rescaling the σ value of oxygen by 1.3. For H_3O^-, we adopted the LJ plus Coulomb parameters proposed by Netz but by rescaling the σ value of oxygen by 0.95. These rescaling factors were obtained after testing several values and they were selected as the best option to better describe hydration free energy of OH^- and H_3O^- at room temperature. Thus, in this work, we proposed the following set of force field parameters: for OH^- ($q_O = -1.28$, $q_H = 0.28$, $\varepsilon_O = 0.251$ kJ/mol, $\varepsilon_H = 0.184$ kJ/mol, $\sigma_O = 0.405$ nm, and $\sigma_H = 0.257$ nm) and for H_3O^- ($q_O = -1.4$, $q_H = 0.8$, $\varepsilon_O = 0.8$ kJ/mol, $\varepsilon_H = 0.0$ kJ/mol, $\sigma_O = 0.295$ nm, and $\sigma_H = 0.0$ nm). For both OH^- and H_3O^-, we adopted the UFF[84] bonded parameters. All QM calculations were performed using the Gaussian 09 package.[85] All information about the geometry of polyatomic ions and force field parameters for all ions used in the simulations is available in the Supporting Information.

■ ASSOCIATED CONTENT

Supporting Information

The Supporting Information is available free of charge at https://pubs.acs.org/doi/10.1021/acs.jctc.1c00116.

More information concerning the force field parameters, radial distribution functions, hydration free-energy terms, single-ion heat of transport, reduced single-ion mass current, effective mass diffusion, thermodiffusion, and salt Soret and Seebeck coefficients (PDF)

https://doi.org/10.1021/acs.jctc.1c00116
J. Chem. Theory Comput. 2021, 17, 3539−3553

AUTHOR INFORMATION

Corresponding Authors

Leandro Rezende Franco − *Universidade de Sao Paulo, Instituto de Fisica, Cidade Universitaria, Sao Paulo 05508-090, SP, Brazil*; Email: leofranc@if.usp.br

André Luiz Sehnem − *Universidade de Sao Paulo, Instituto de Fisica, Cidade Universitaria, Sao Paulo 05508-090, SP, Brazil*; orcid.org/0000-0002-3544-2277; Email: alsehnem@if.usp.br

Antônio Martins Figueiredo Neto − *Universidade de Sao Paulo, Instituto de Fisica, Cidade Universitaria, Sao Paulo 05508-090, SP, Brazil*; orcid.org/0000-0002-6339-8699; Email: afigueiredo@if.usp.br

Kaline Coutinho − *Universidade de Sao Paulo, Instituto de Fisica, Cidade Universitaria, Sao Paulo 05508-090, SP, Brazil*; orcid.org/0000-0002-7586-3324; Email: kaline@if.usp.br

Complete contact information is available at: https://pubs.acs.org/10.1021/acs.jctc.1c00116

Notes

The authors declare no competing financial interest.

ACKNOWLEDGMENTS

The authors thank the National Institute of Science and Technology of Complex Fluids (INCT-FCx) for the CNPq grant 141260/2017-3 and FAPESP grant 2014/50983-3; CAPES concerning the BioMol project 23038.004630/2014-35; FAPESP grants 2017/11631-2, 2019/10433-8, and 2016/24531-3; and High Performance Computing of USP (HPC-USP) for computational resources.

REFERENCES

(1) Zhao, D.; Wang, H.; Khan, Z. U.; Chen, J. C.; Gabrielsson, R.; Jonsson, M. P.; Berggren, M.; Crispin, X. Ionic thermoelectric supercapacitors. *Energy Environ. Sci.* **2016**, *9*, 1450−1457.

(2) Li, T.; Zhang, X.; Lacey, S. D.; Mi, R.; Zhao, X.; Jiang, F.; Song, J.; Liu, Z.; Chen, G.; Dai, J.; Yao, Y.; Das, S.; Yang, R.; Briber, R. M.; Hu, L. Cellulose ionic conductors with high differential thermal voltage for low-grade heat harvesting. *Nat. Mater.* **2019**, *18*, 608.

(3) Bonetti, M.; Nakamae, S.; Roger, M.; Guenoun, P. Huge Seebeck coefficients in nonaqueous electrolytes. *J. Chem. Phys.* **2011**, *134*, 114513.

(4) Kim, H. S.; Liu, W.; Chen, G.; Chu, C.-W.; Ren, Z. Relationship between thermoelectric figure of merit and energy conversion efficiency. *Proc. Natl. Acad. Sci. U.S.A.* **2015**, *112*, 8205−8210.

(5) Bonetti, M.; Nakamae, S.; Huang, B. T.; Salez, T. J.; Wiertel-Gasquet, C.; Roger, M. Thermoelectric energy recovery at ionic-liquid/electrode interface. *J. Chem. Phys.* **2015**, *142*, 244708.

(6) Köhler, W.; Morozov, K. I. The Soret Effect in Liquid Mixtures − A Review. *J. Non-Equilib. Thermodyn.* **2016**, *41*, 151−197.

(7) Würger, A. Thermal non-equilibrium transport in colloids. *Rep. Prog. Phys.* **2010**, *73*, 126601.

(8) Agar, J. N.; Mou, C. Y.; Lin, J. L. Single-ion heat of transport in electrolyte solutions: a hydrodynamic theory. *J. Phys. Chem.* **1989**, *93*, 2079−2082.

(9) Zhao, D.; Martinelli, A.; Willfahrt, A.; Fischer, T.; Bernin, D.; Khan, Z. U.; Shahi, M.; Brill, J.; Jonsson, M. P.; Fabiano, S.; Crispin, X. Polymer gels with tunable ionic Seebeck coefficient for ultra-sensitive printed thermopiles. *Nat. Commun.* **2019**, *10*, 1093.

(10) Ludwig, C. *Diffusion zwischen ungleich erwrmten orten gleich zusammengesetzter lsungen*; Sitzungsber. Adad. Wiss. Wien, 1856; Vol. *20*; p 539.

(11) Soret, C. Concentrations differentes d'une dissolution dont deux parties sont à des températures différéntes. *Arch. Sci. Phys. Nat.* **1879**, *2*, 48−61.

(12) Eastman, E. D. Theory of the Soret effect. *J. Am. Chem. Soc.* **1928**, *50*, 283−291.

(13) Eastman, E. D. The Thermodynamics of Non-Isothermal Systems. *J. Am. Chem. Soc.* **1927**, *49*, 794−795.

(14) Agar, J. N.; Turner, J. C. R. Thermal Diffusion in Solutions of Electrolytes. *Proc. R. Soc. London, Ser. A* **1960**, *255*, 307−330.

(15) Agar, J. N. Thermogalvanic Cells, in Advances in Electrochemistry and Electrochemical Engineering. *Advances in Electrochemistry and Electrochemical Engineering*; Interscience: New York, 1963; pp 31−121.

(16) Römer, F.; Wang, Z.; Wiegand, S.; Bresme, F. Alkali Halide Solutions under Thermal Gradients: Soret Coefficients and Heat Transfer Mechanisms. *J. Phys. Chem. B* **2013**, *117*, 8209−8222.

(17) Eslahian, K. A.; Maskos, M. Hofmeister effect in thermal field-flow fractionation of colloidal aqueous dispersions. *Colloids Surf., A* **2012**, *413*, 65−70.

(18) Eslahian, K. A.; Majee, A.; Maskos, M.; Würger, A. Specific salt effects on thermophoresis of charged colloids. *Soft Matter* **2014**, *10*, 1931−1936.

(19) Niether, D.; Kawaguchi, T.; Hovancová, J.; Eguchi, K.; Dhont, J. K. G.; Kita, R.; Wiegand, S. Role of Hydrogen Bonding of Cyclodextrin-Drug Complexes Probed by Thermodiffusion. *Langmuir* **2017**, *33*, 8483−8492.

(20) Niether, D.; Kriegs, H.; Dhont, J. K. G.; Wiegand, S. Peptide model systems: Correlation between thermophilicity and hydrophilicity. *J. Chem. Phys.* **2018**, *149*, 044506.

(21) Stout, R. F.; Khair, A. S. Diffuse charge dynamics in ionic thermoelectrochemical systems. *Phys. Rev. E* **2017**, *96*, 022604.

(22) Janssen, M.; Bier, M. Transient response of an electrolyte to a thermal quench. *Phys. Rev. E* **2019**, *99*, 042136.

(23) Reichl, M.; Herzog, M.; Gatz, A.; Braun, D. Why Charged Molecules Move Across a Temperature Gradient: The Role of Electric Fields. *Phys. Rev. Lett.* **2014**, *112*, 198101.

(24) Sehnem, A. L.; Figueiredo Neto, A. M.; Aquino, R.; Campos, A. F. C.; Tourinho, F. A.; Depeyrot, J. Temperature dependence of the Soret coefficient of ionic colloids. *Phys. Rev. E* **2015**, *92*, 042311.

(25) Sehnem, A. L.; Neto, A. M. F.; Niether, D.; Wiegand, S. Diffusiophoresis as Ruling Effect: Influence of Organic Salts on Thermodiffusion of Iron Oxide Nanoparticles. *Phys. Rev. E* **2018**, *98*, 062615.

(26) Huang, B. T.; Roger, M.; Bonetti, M.; Salez, T. J.; Wiertel-Gasquet, C.; Dubois, E.; Gomes, R. C.; Demouchy, G.; Mériguet, G.; Peyre, V.; Kouyaté, M.; Filomeno, C. L.; Depeyrot, J.; Tourinho, F. A.; Perzynski, R.; Nakamae, S. Thermoelectricity and thermodiffusion in charged colloids. *J. Chem. Phys.* **2015**, *143*, 054902.

(27) Salez, T. J.; Huang, B. T.; Rietjens, M.; Bonetti, M.; Wiertel-Gasquet, C.; Roger, M.; Filomeno, C. L.; Dubois, E.; Perzynski, R.; Nakamae, S. Can charged colloidal particles increase the thermoelectric energy conversion efficiency? *Phys. Chem. Chem. Phys.* **2017**, *19*, 9409−9416.

(28) Duhr, S.; Braun, D. Why molecules move along a temperature gradient. *Proc. Natl. Acad. Sci. U.S.A.* **2006**, *103*, 19678−19682.

(29) Astumian, R. D. Coupled transport at the nanoscale: The unreasonable effectiveness of equilibrium theory. *Proc. Natl. Acad. Sci. U.S.A.* **2007**, *104*, 3−4.

(30) Würger, A. Is Soret equilibrium a non-equilibrium effect? *C. R. Mec.* **2013**, *341*, 438−448. , 10th International Meeting on Thermodiffusion

(31) Takeyama, N.; Nakashima, K. Proportionality of Intrinsic Heat of Transport to Standard Entropy of Hydration for Aqueous Ions. *J. Solution Chem.* **1988**, *17*, 305−325.

(32) Carlsson, J.; Åqvist, J. Absolute Hydration Entropies of Alkali Metal Ions from Molecular Dynamics Simulations. *J. Phys. Chem. B* **2009**, *113*, 10255−10260.

(33) Niether, D.; Kriegs, H.; Dhont, J. K. G.; Wiegand, S. Peptide model systems: Correlation between thermophilicity and hydrophilicity. *J. Chem. Phys.* **2018**, *149*, 044506.
(34) Niether, D.; Di Lecce, S.; Bresme, F.; Wiegand, S. Unravelling the hydrophobicity of urea in water using thermodiffusion: implications for protein denaturation. *Phys. Chem. Chem. Phys.* **2018**, *20*, 1012−1020.
(35) Di Lecce, S.; Albrecht, T.; Bresme, F. A computational approach to calculate the heat of transport of aqueous solutions. *Sci. Rep.* **2017**, *7*, 44833.
(36) Di Lecce, S.; Bresme, F. Soret coefficients and thermal conductivities of alkali halide aqueous solutions via non-equilibrium molecular dynamics simulations. *Mol. Simul.* **2019**, *45*, 351−357.
(37) Astumian, R. D. The unreasonable effectiveness of equilibrium theory for interpreting nonequilibrium experiments. *Am. J. Phys.* **2006**, *74*, 683−688.
(38) Schmid, R.; Miah, A. M.; Sapunov, V. N. A new table of the thermodynamic quantities of ionic hydration: values and some applications (enthalpy-entropy compensation and Born radii). *Phys. Chem. Chem. Phys.* **2000**, *2*, 97−102.
(39) Marcus, Y. A simple empirical model describing the thermodynamics of hydration of ions of widely varying charges, sizes, and shapes. *Biophys. Chem.* **1994**, *51*, 111−127.
(40) Pliego, J. R., Jr; Riveros, J. M. New values for the absolute solvation free energy of univalent ions in aqueous solution. *Chem. Phys. Lett.* **2000**, *332*, 597−602.
(41) Light, T. S.; Licht, S.; Bevilacqua, A. C.; Morash, K. R. The fundamental conductivity and resistivity of water. *Electrochem. Solid-State Lett.* **2005**, *8*, No. E16.
(42) Sehnem, A. L.; Niether, D.; Wiegand, S.; Figueiredo Neto, A. M. Thermodiffusion of Monovalent Organic Salts in Water. *J. Phys. Chem. B* **2018**, *122*, 4093−4100.
(43) Sehnem, A. L.; Neto, A. M. F. Dynamic Response of a Thermoelectric Cell Induced by Ion Thermodiffusion. **2019**, arXiv:1911.11799.
(44) Canongia Lopes, J. N.; Deschamps, J.; Pádua, A. A. H. Modeling ionic liquids using a systematic all-atom force field. *J. Phys. Chem. B* **2004**, *108*, 2038−2047.
(45) Smith, D. E.; Dang, L. X. Computer simulations of NaCl association in polarizable water. *J. Chem. Phys.* **1994**, *100*, 3757−3766.
(46) Jensen, K. P.; Jorgensen, W. L. Halide, ammonium, and alkali metal ion parameters for modeling aqueous solutions. *J. Chem. Theory Comput.* **2006**, *2*, 1499−1509.
(47) Roux, B. Valence selectivity of the gramicidin channel: a molecular dynamics free energy perturbation study. *Biophys. J.* **1996**, *71*, 3177−3185.
(48) Åqvist, J. Ion-water interaction potentials derived from free energy perturbation simulations. *J. Phys. Chem.* **1990**, *94*, 8021−8024.
(49) Dang, L. X.; Kollman, P. A. Free Energy of Association of the K +:18-Crown-6 Complex in Water: A New Molecular Dynamics Study. *J. Phys. Chem.* **1995**, *99*, 55−58.
(50) Beglov, D.; Roux, B. Finite representation of an infinite bulk system: solvent boundary potential for computer simulations. *J. Chem. Phys.* **1994**, *100*, 9050−9063.
(51) Bonthuis, D. J.; Mamatkulov, S. I.; Netz, R. R. Optimization of classical nonpolarizable force fields for OH− and H3O+. *J. Chem. Phys.* **2016**, *144*, 104503.
(52) Ufimtsev, I. S.; Kalinichev, A. G.; Martinez, T. J.; Kirkpatrick, R. J. A charged ring model for classical OH−(aq) simulations. *Chem. Phys. Lett.* **2007**, *442*, 128−133.
(53) Berg, H. *Random Walks in Biology*; Princeton University Press, 1983.
(54) Day, T. J. F.; Soudackov, A. V.; Čuma, M.; Schmitt, U. W.; Voth, G. A. A second generation multistate empirical valence bond model for proton transport in aqueous systems. *J. Chem. Phys.* **2002**, *117*, 5839−5849.
(55) Lee, S. H.; Rasaiah, J. C. Proton transfer and the mobilities of the H+ and OH− ions from studies of a dissociating model for water. *J. Chem. Phys.* **2011**, *135*, 124505.
(56) Ojamäe, L.; Shavitt, I.; Singer, S. J. Potential models for simulations of the solvated proton in water. *J. Chem. Phys.* **1998**, *109*, 5547−5564.
(57) Bringuier, E. On the notion of thermophoretic velocity. *Philos. Mag.* **2007**, *87*, 873−883.
(58) De Groot, S. R. Sur la thermodynamique de quelques processus irréversibles. II. Diffusion thermique et phénomènes connexes. *J. Phys. Radium* **1947**, *8*, 193−200.
(59) Sehnem, A. L.; Janssen, M. Determining Single-Ion Soret Coefficients from the Transient Electrolyte Seebeck Effect. **2020**, https://arxiv.org/pdf/2006.11081.
(60) Wang, H.; Zhao, D.; Khan, Z. U.; Puzinas, S.; Jonsson, M. P.; Berggren, M.; Crispin, X. Ionic Thermoelectric Figure of Merit for Charging of Supercapacitors. *Adv. Electron. Mater.* **2017**, *3*, 1700013.
(61) Van Der Spoel, D.; Lindahl, E.; Hess, B.; Groenhof, G.; Mark, A. E.; Berendsen, H. J. C. GROMACS: fast, flexible, and free. *J. Comput. Chem.* **2005**, *26*, 1701−1718.
(62) Wu, X.; Brooks, B. R. Self-guided Langevin dynamics simulation method. *Chem. Phys. Lett.* **2003**, *381*, 512−518.
(63) Bussi, G.; Donadio, D.; Parrinello, M. Canonical sampling through velocity rescaling. *J. Chem. Phys.* **2007**, *126*, 014101.
(64) Berendsen, H. J. C.; Postma, J. P. M.; van Gunsteren, W. F.; DiNola, A.; Haak, J. R. Molecular dynamics with coupling to an external bath. *J. Chem. Phys.* **1984**, *81*, 3684−3690.
(65) Essmann, U.; Perera, L.; Berkowitz, M. L.; Darden, T.; Lee, H.; Pedersen, L. G. A smooth particle mesh Ewald method. *J. Chem. Phys.* **1995**, *103*, 8577−8593.
(66) Hockney, R. W.; Goel, S. P.; Eastwood, J. W. Quiet high-resolution computer models of a plasma. *J. Comput. Phys.* **1974**, *14*, 148−158.
(67) Van Gunsteren, W. F.; Berendsen, H. J. C. A leap-frog algorithm for stochastic dynamics. *Mol. Simul.* **1988**, *1*, 173−185.
(68) Goga, N.; Rzepiela, A. J.; De Vries, A. H.; Marrink, S. J.; Berendsen, H. J. C. Efficient algorithms for Langevin and DPD dynamics. *J. Chem. Theory Comput.* **2012**, *8*, 3637−3649.
(69) Hess, B.; Bekker, H.; Berendsen, H. J. C.; Fraaije, J. G. E. M. LINCS: a linear constraint solver for molecular simulations. *J. Comput. Chem.* **1997**, *18*, 1463−1472.
(70) Bennett, C. H. Efficient estimation of free energy differences from Monte Carlo data. *J. Comput. Phys.* **1976**, *22*, 245−268.
(71) Frenkel, D.; Smit, B. *Understanding Molecular Simulation*; Academic Press: San Diego, 1996; pp 27−33.
(72) Berendsen, H. J. C.; Grigera, J. R.; Straatsma, T. P. The missing term in effective pair potentials. *J. Phys. Chem.* **1987**, *91*, 6269.
(73) Jorgensen, W. L.; Chandrasekhar, J.; Madura, J. D.; Impey, R. W.; Klein, M. L. Comparison of simple potential functions for simulating liquid water. *J. Chem. Phys.* **1983**, *79*, 926−935.
(74) Jorgensen, W. L.; Maxwell, D. S.; Tirado-Rives, J. Development and testing of the OPLS all-atom force field on conformational energetics and properties of organic liquids. *J. Am. Chem. Soc.* **1996**, *118*, 11225−11236.
(75) Kaminski, G. A.; Friesner, R. A.; Tirado-Rives, J.; Jorgensen, W. L. Evaluation and Reparametrization of the OPLS-AA Force Field for Proteins via Comparison with Accurate Quantum Chemical Calculations on Peptides†. *J. Phys. Chem. B* **2001**, *105*, 6474−6487.
(76) Breneman, C. M.; Wiberg, K. B. Determining atom-centered monopoles from molecular electrostatic potentials. The need for high sampling density in formamide conformational analysis. *J. Comput. Chem.* **1990**, *11*, 361−373.
(77) Scalmani, G.; Frisch, M. J. Continuous surface charge polarizable continuum models of solvation. I. General formalism. *J. Chem. Phys.* **2010**, *132*, 114110.
(78) Head-Gordon, M.; Pople, J. A.; Frisch, M. J. MP2 energy evaluation by direct methods. *Chem. Phys. Lett.* **1988**, *153*, 503−506.
(79) Dunning, T. H., Jr Gaussian basis sets for use in correlated molecular calculations. I. The atoms boron through neon and hydrogen. *J. Chem. Phys.* **1989**, *90*, 1007−1023.

https://doi.org/10.1021/acs.jctc.1c00116
J. Chem. Theory Comput. 2021, 17, 3539−3553

(80) Franco, L. R.; Brandão, I.; Fonseca, T. L.; Georg, H. C. Elucidating the structure of merocyanine dyes with the ASEC-FEG method. Phenol blue in solution. *J. Chem. Phys.* **2016**, *145*, 194301.
(81) Brandão, I.; Franco, L. R.; Fonseca, T. L.; Castro, M. A.; Georg, H. C. Confirming the relationship between first hyperpolarizability and the bond length alternation coordinate for merocyanine dyes. *J. Chem. Phys.* **2017**, *146*, 224505.
(82) Cezar, H. M.; Canuto, S.; Coutinho, K. Solvent effect on the syn/anti conformational stability: A comparison between conformational bias Monte Carlo and molecular dynamics methods. *Int. J. Quantum Chem.* **2019**, *119*, No. e25688.
(83) Krishnan, R.; Pople, J. A. Approximate fourth-order perturbation theory of the electron correlation energy. *Int. J. Quantum Chem.* **1978**, *14*, 91−100.
(84) Garberoglio, G. OBGMX: A web-based generator of GROMACS topologies for molecular and periodic systems using the universal force field. *J. Comput. Chem.* **2012**, *33*, 2204−2208.
(85) Frisch, M. J.; Trucks, G. W.; Schlegel, H. B.; Scuseria, G. E.; Robb, M. A.; Cheeseman, J. R.; Scalmani, G.; Barone, V.; Mennucci, B.; Petersson, G. A.; Nakatsuji, H.; Caricato, M.; Li, X.; Hratchian, H. P.; Izmaylov, A. F.; Bloino, J.; Zheng, G.; Sonnenberg, J. L.; Hada, M.; Ehara, M.; Toyota, K.; Fukuda, R.; Hasegawa, J.; Ishida, M.; Nakajima, T.; Honda, Y.; Kitao, O.; Nakai, H.; Vreven, T.; Montgomery, J. A., Jr.; Peralta, J. E.; Ogliaro, F.; Bearpark, M.; Heyd, J. J.; Brothers, E.; Kudin, K. N.; Staroverov, V. N.; Kobayashi, R.; Normand, J.; Raghavachari, K.; Rendell, A.; Burant, J. C.; Iyengar, S. S.; Tomasi, J.; Cossi, M.; Rega, N.; Millam, J. M.; Klene, M.; Knox, J. E.; Cross, J. B.; Bakken, V.; Adamo, C.; Jaramillo, J.; Gomperts, R.; Stratmann, R. E.; Yazyev, O.; Austin, A. J.; Cammi, R.; Pomelli, C.; Ochterski, J. W.; Martin, R. L.; Morokuma, K.; Zakrzewski, V. G.; Voth, G. A.; Salvador, P.; Dannenberg, J. J.; Dapprich, S.; Daniels, A. D.; Farkas, O.; Foresman, J. B.; Ortiz, J. V.; Cioslowski, J.; Fox, D. J. *Gaussian 09*, Revision D.01; Gaussian, Inc.: Wallingford, CT, 2013.

https://doi.org/10.1021/acs.jctc.1c00116
J. Chem. Theory Comput. 2021, 17, 3539−3553